



TRC1102

**Slope Stability Monitoring  
Using Remote Sensing Technologies**

Richard A. Coffman, Omar A. Conte

Final Report

2014

FINAL REPORT: AHTD TRC-1102

SLOPE STABILITY MONITORING USING REMOTE SENSING TECHNIQUES

Submitted By:

Richard A. Coffman, PhD, PE, PLS  
Assistant Professor  
Department of Civil Engineering  
4190 Bell Engineering Center  
Fayetteville, AR 72701

Omar A. Conte, MSCE, EIT  
(former Graduate Student at the University of Arkansas)  
Fugro Panama, SA  
Ciudad del Saber, Clayton  
Edificio 141, Calle Gustavo Lara  
Panama, Rep. de Panama

## **Abstract**

Two slope failures that affected Interstates in the state of Arkansas were monitored using traditional surveying techniques (total station) and advanced remote sensing techniques (Light Detection And Ranging [LiDAR] and Radio Detection and Ranging [RADAR]). One site (calibration site) was located near Chester, Arkansas, and the other slope failure (validation site) was located near Malvern, Arkansas. The results of monitoring program, slope stability analysis, geotechnical exploration and laboratory testing program conducted at both sites (calibration and validation) are discussed and compared in this final report.

## Table of Contents

<b>Abstract</b> .....	<b>ii</b>
<b>Table of Contents</b> .....	<b>iii</b>
<b>List of Figures</b> .....	<b>v</b>
<b>List of Tables</b> .....	<b>viii</b>
<b>List of Equations</b> .....	<b>ix</b>
<b>Chapter 1 . Introduction</b> .....	<b>1</b>
<b>Chapter 2 . Calibration Site Near Chester, Arkansas</b> .....	<b>2</b>
2.1 . <i>Introduction</i> .....	2
2.2 . <i>Location of the Calibration Site</i> .....	2
2.3 . <i>Data Acquisition and Limit Equilibrium Analyses at the Calibration Site</i> .....	4
2.3.1 . <i>Total Station</i> .....	4
2.3.2 . <i>LIDAR</i> .....	5
2.3.3 . <i>RADAR</i> .....	6
2.3.4 . <i>Limit Equilibrium Slope Stability Analyses</i> .....	8
2.4 . <i>Results Obtained from the Calibration Site</i> .....	8
2.4.1 . <i>Total Station</i> .....	9
2.4.2 . <i>LIDAR</i> .....	12
2.4.3 . <i>RADAR</i> .....	14
2.4.4 . <i>Limit Equilibrium Slope Stability Analyses</i> .....	15
<b>Chapter 3 . Validation Site Near Malvern, Arkansas</b> .....	<b>18</b>
3.1 . <i>Introduction</i> .....	18
3.2 . <i>Validation Site Overview</i> .....	18
3.3 . <i>Data Acquisition at the Validation Site</i> .....	19
3.3.1 . <i>Total Station</i> .....	20
3.3.2 . <i>LIDAR</i> .....	21
3.3.3 . <i>RADAR</i> .....	21
3.3.4 . <i>Geotechnical Exploration</i> .....	22
3.3.5 . <i>Limit Equilibrium Slope Stability Analyses</i> .....	23
3.4 . <i>Results Obtained from the Validation Site</i> .....	24
3.4.1 . <i>Total Station</i> .....	24

3.4.2 . <i>LIDAR</i> .....	24
3.4.3 . <i>RADAR</i> .....	25
3.4.4 . <i>Geotechnical Exploration</i> .....	26
3.4.5 . <i>Limit Equilibrium Slope Stability Analyses</i> .....	36
<b>Chapter 4 . Conclusions</b> .....	<b>44</b>
<b>Chapter 5 . References</b> .....	<b>45</b>
<b>Appendix A . LAsTools©</b> .....	<b>46</b>

## List of Figures

Figure 2.1. Location of calibration site along Interstate 540, near Log Mile 36.4 North of Chester, AR (Google Maps, 2011). .....	2
Figure 2.2. Photograph obtained while looking northeast across southbound lane of I-540 at calibration site near Chester, Arkansas. ....	3
Figure 2.3. a) Looking north, the main scarp at the calibration site located in Chester, Arkansas, and b) tension crack observed in the median of I-540. ....	3
Figure 2.4. Plan view of calibration near Chester, Arkansas; the locations of survey monuments are illustrated. ....	4
Figure 2.5. a) Nikon DTM-520 (Nikon Positioning Website, 2012), b) Optima 30mm prism, c) flat shoe for prism pole, and d) pointed shoe on the prim pole. ....	5
Figure 2.6. a) RADAR and LIDAR Southbound viewpoint, and b) LIDAR deployed at Point 2010. ....	5
Figure 2.7. GPRI-II features (from GAMMA Remote Sensing AG, 2011). ....	7
Figure 2.8. a) Placing concrete footings for GPRI-II at the Southbound viewpoint at the calibration site, and b) tripod of GPRI-II anchored at the Southbound viewpoint near Chester, Arkansas. ....	8
Figure 2.9. Horizontal displacements measured and precipitation data for calibration site. ....	10
Figure 2.10. Elevation differences measured and precipitation data for calibration site. ....	10
Figure 2.11. Displacement areas for the calibration site; different colors represent the different displacement intervals [in color]. ....	11
Figure 2.12. Zones of vertical movements for the calibration site; red zone represents largest down movements, orange zone represents down medium movements, yellow areas low to zero down movement, and blue areas represent uplift movement [in color]. ....	12
Figure 2.13. a) Volume surface 03/17/11 to 06/08/11 (obtained using bare earth correction method) where maximum elevation difference on the main scarp was observed, and b) zoomed view to the main scarp where progressive movement was observed from 05/17/11 to 06/08/11 [in color]. ....	13
Figure 2.14. a) MLI RADAR image obtained from southbound viewpoint in polar corrdinates using 250ms chirp, and b) MLI RADAR image obtained from southbound viewpoint in rectangular corrdinates using 250ms chirp. ....	14
Figure 2.15. a) Southbound viewpoint interferogram from 03/08/11 to 03/26/11, and b) southbound viewpoint interferogram from 03/08/11 to 02/26/12. ....	15

Figure 2.16. Computed UARK slip surfaces using SLIDE 5.044 (2010).....	17
Figure 3.1. Location of project site located at Log Mile 95.7 on Interstate 30 near Malvern, Arkansas. Anticipated slide area shaded in red (Google Maps, 2011). .....	19
Figure 3.2. a) Looking southwest from the hillside between Highway 84 and I-30, and b) looking west towards I-30 at the validation site near Malvern, Arkansas in December 2010.....	19
Figure 3.3. a) Installation of survey monument in the ground by UofA and AHTD personnel, and b) survey monument installed in the ground using Quickcrete®. ....	20
Figure 3.4. Plan view of survey monument positions installed in validation site near Malvern, Arkansas.....	21
Figure 3.5. Geotechnical investigation borehole locations at the validation site (modified from Google Maps, 2011).....	23
Figure 3.6. a) Volume surface (062711-080111) using bare earth correction method, and b) volume surface (062711-120211) using bare earth correction method [in color]. ....	25
Figure 3.7. Profile of the slope inclinometer installed at B-1 location for the site visits to the validation site, and b) Profile of the slope inclinometers casing installed at the B-3 location for the site visits to the validation site. ....	28
Figure 3.8. Profile of the slope inclinometer installed at B-4 location for the site visits to the validation site, and b) Profile of the slope inclinometers casing installed at the B-6 location for the site visits to the validation site. ....	29
Figure 3.9. Sliding surface as recorded by slope inclinometers installed at validation site [in color].....	30
Figure 3.10. Design moisture content, unit weight and Atterberg Limits profile.....	31
Figure 3.11. Pressure obtained from the nested vibrating wire piezometer [in color].....	33
Figure 3.12. Design strength profile for validation site near Malvern, Arkansas.....	34
Figure 3.13. Normalized stress-strain graph of UU test for B-2 specimens at validation site.....	35
Figure 3.14. Preliminary slope stability model for validation site using UARK correlation. ....	39
Figure 3.15. Refined slope stability model for validation site using UARK correlation.....	42
Figure 3.16. Refined slope stability model for validation site using UU test results (residual undrained strength). ....	43
Figure A.1. Point cloud for Chester site in Leica Geosystems Cyclone software suite. ....	47

Figure A.2. Unified point cloud (.las) as viewed in lastools lasview.exe.....	48
Figure A.3. Both vegetation and non-vegetative points. ....	48
Figure A.4. Ground point cloud after separation. ....	49
Figure A.5. Vegetation points after separation .....	49
Figure A.6. Ground point cloud after thinning. ....	50

## List of Tables

Table 2.1. Summary of soil parameters used in the slope stability analysis for calibration site ..	16
Table 2.2. Summary of factors of safety obtained using different SPT- $S_u$ correlation methods for calibration site.....	16
Table 3.1. Summary of results for inclinometers installed at validation site.....	27
Table 3.2. Summary of the initial soil parameters utilized in the initial slope stability analysis for the validation site. ....	38
Table 3.3. Summary of results for the preliminary slope stability analysis of the validation site.	38
Table 3.4. Summary of the refined soil parameters used in the refined slope stability analysis at the validation site near Malvern, Arkansas.....	40
Table 3.5. Summary of factors of safety obtained after refined slope stability analysis for the validation site.....	41

## List of Equations

Equation 2.1.....	8
-------------------	---

## **Chapter 1. Introduction**

While individual slope failures are not as spectacular or costly as other natural disasters such as earthquakes, major floods, and tornadoes; slope failures are more widespread. In aggregate, the total financial loss due to slope failures is probably greater than that for any other single geologic hazard (Griffiths et al., 1999). The ability to precisely identify the extents of landslide, and to monitor and pre-emptively mitigate potential landslide disasters can help save money and ensure slope remediation is properly performed. The hypothesis is that the use of remote sensing techniques saves labor time and equipment cost when used on numerous projects relative to the current state of practice (inclinometers, piezometers, traditional survey measurements).

During the past eight years the Arkansas State Highway and Transportation Department (AHTD) has spent over nine million US dollars repairing slope failures that have occurred in the state of Arkansas. Therefore the necessity to quantitatively identify the surface extents, movement rates, vertical displacements, and direction of movements for a given landslide using advanced remote sensing techniques exists. Specifically, the Gamma Portable RADAR Interferometer (GPRI-II) and a Leica C-10 Light Detection and Ranging (LIDAR) were investigated as devices that would enable collection of data that would facilitate detection of slope failure locations. Furthermore, it was investigated if the results obtained from these advanced remote sensing techniques (LIDAR and GPRI) were more precise than the commonly employed traditional surveying techniques and if the results obtained from the advanced remote sensing techniques were comparable to results obtained by using standard monitoring techniques such as slope inclinometers and piezometers.

## Chapter 2. Calibration Site Near Chester, Arkansas

### 2.1. Introduction

The slope failure that occurred at the calibration site located near Chester, Arkansas, was partially discussed and presented in Conte and Coffman (2012), where the results from the LIDAR monitoring program and the limit equilibrium slope stability results were presented. Therefore, for brevity, the background information and details for this site are only briefly discussed. However, a more robust method to process the LIDAR data (bare earth correction) is presented herein, and the results for the total station and RADAR are summarized and discussed.

### 2.2. Location of the Calibration Site

The slide that occurred near Chester, Arkansas, on Interstate 540, near Log Mile 36.4 (Figure 2.1) is approximately 2.5 miles north of the town center of Chester, Arkansas. The site is located approximately 36 miles from the University of Arkansas Bell Engineering Center and five miles South of the Bobby Hopper tunnel. The driving time from the University to this project site was approximately 30 minutes.



**Figure 2.1. Location of calibration site along Interstate 540, near Log Mile 36.4, North of Chester, AR (Google Maps, 2011).**

The location of the calibration site was ideal for research operations due to the lack of population in the area where the slide was located; however, the slope failure was located in the median of I-540, a major transportation artery in Northwest Arkansas. The surface extents of the study area was approximately 550 feet long (in the direction of the roadway) and extend from the West shoulder of the Northbound lanes to the East shoulder of the Southbound lanes (transverse to the roadway). Pictures of the calibration site, as obtained during the first site visit conducted by University personnel are presented in Figure 2.2 and Figure 2.3.

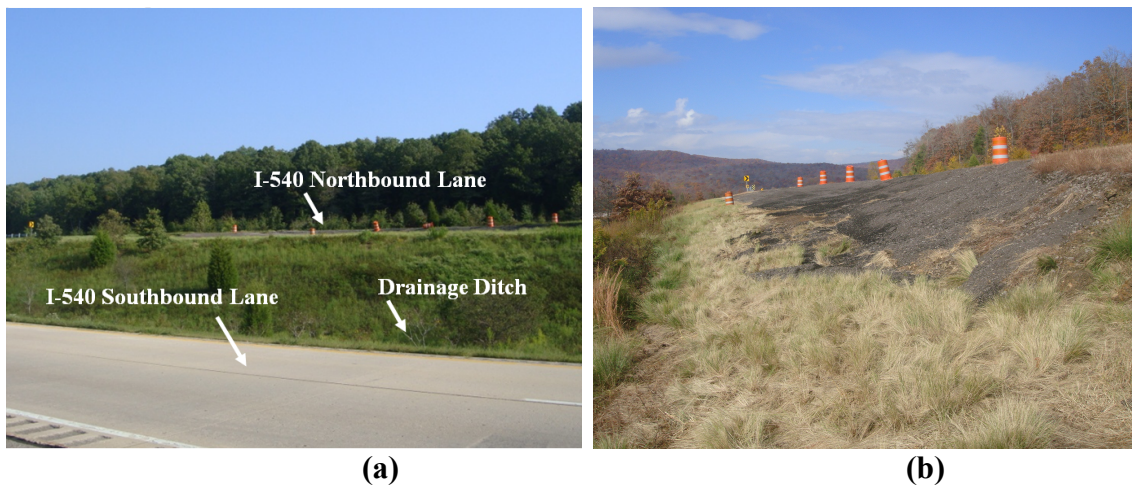


**Figure 2.2. Photograph obtained while looking Northeast across the Southbound lane of I-540 at calibration site near Chester, Arkansas.**

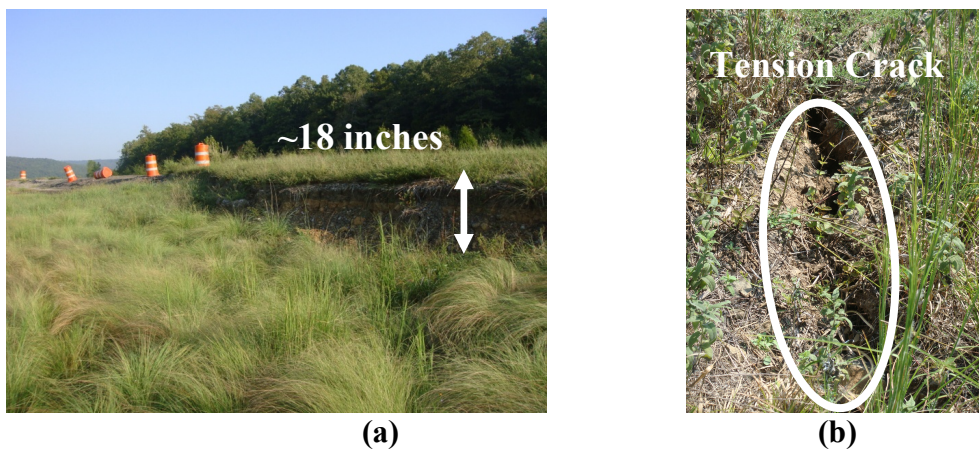


**Figure 2.3. a) Looking north, the main scarp at the calibration site located in Chester, Arkansas, and b) a tension crack observed in the median of I-540.**

### 2.3. Data Acquisition and Limit Equilibrium Analyses at the Calibration Site

Three methods were utilized to acquire data at the calibration site. The three methods consisted of total station, LIDAR, and RADAR. Each of the methods are discussed in the subsequent sections. Limit equilibrium slope stability analyses were also performed to determine if the measured and predicted slope movements coincided.

#### 2.3.1. Total Station

To monitor the site using traditional surveying techniques, this site was instrumented with 29 (Figure 2.4) concrete monuments that encased aluminum surveying monuments mounted on rebar. These monuments served as check points. Each monument consists of a Quikrete® filled borehole (18 inches deep, 3 inches in diameter), a 24-inch long half-inch diameter rebar, and a 2-inch diameter aluminum monument (Conte, 2012). These monuments were monitored every two weeks or after a period of heavy rain. A topographic survey and the monitoring checks were performed using: a Nikon DTM-520 total station, a Leica tripod, a Carlson Explorer 600+ data collector, a Sokkia prism pole with bipod legs, and a Optima 30mm offset prism (Figure 2.5).

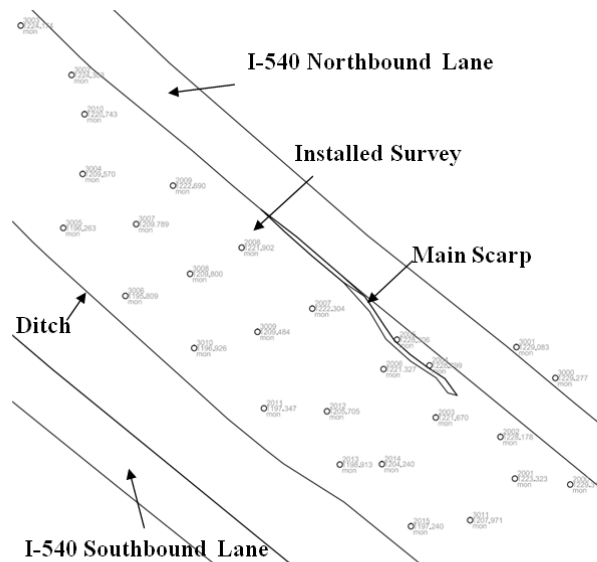


Figure 2.4. Plan view of calibration near Chester, Arkansas; the locations of survey monuments are illustrated.

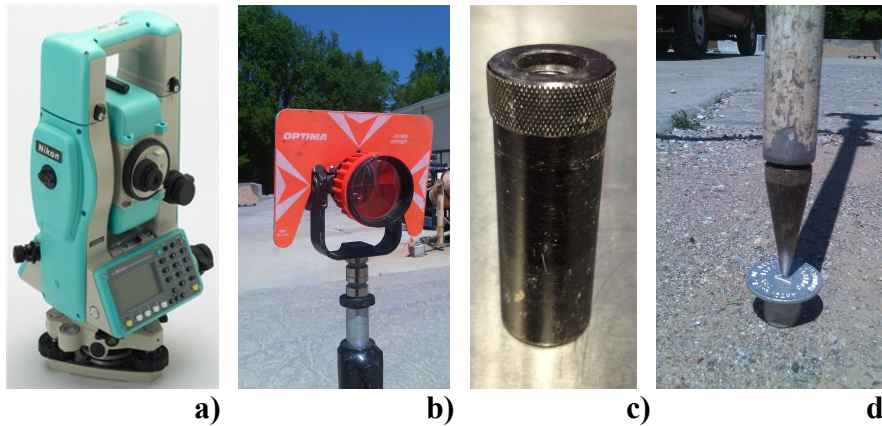


Figure 2.5. a) Nikon DTM-520 (Nikon Positioning Website, 2012), b) Optima 30mm prism, c) flat shoe for prism pole, and d) pointed shoe on the prim pole.

### 2.3.2. LIDAR

Ground based LIDAR equipment has been used for landslide monitoring during the last decade because of the high accuracy and high portability. The LIDAR used in this research project was a Leica C-10. According to the (Leica, 2011), the maximum range of this instrument is 984 ft. (300 m.) at 90% albedo, with a resolution of 7mm (Gaussian-based) and wavelength of 532 nm. Scans (360 degree) were performed at each viewpoint using the LIDAR. Additional targets were utilized at the AHTD control points, or benchmarks, to tie the scans to geographical coordinates. The two LIDAR locations utilized at the calibration site are presented in Figure 2.6.

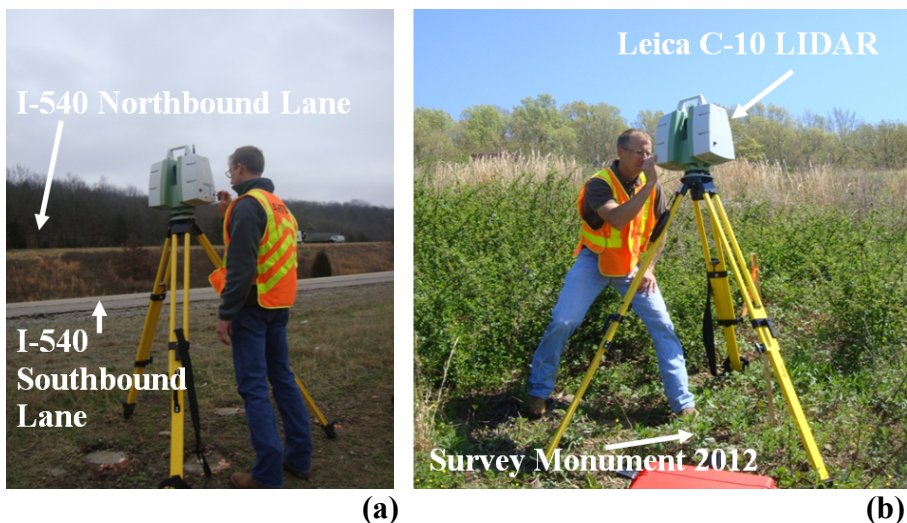
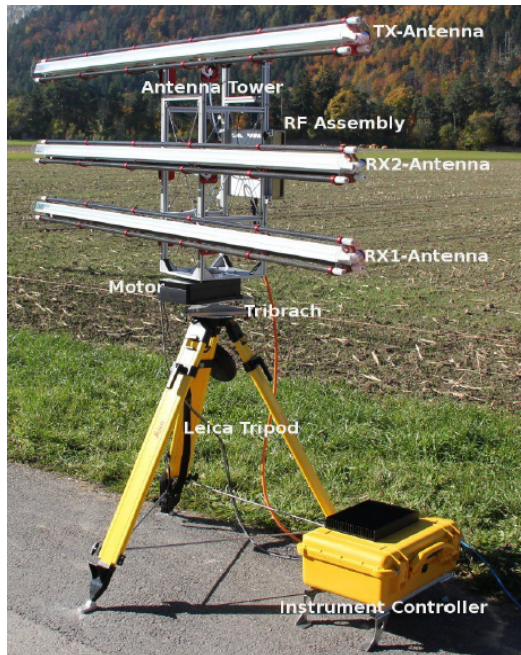


Figure 2.6. a) RADAR and LIDAR Southbound viewpoint, and b) LIDAR deployed at Point 2012.

LIDAR scans were performed once a month, by AHTD personnel, at the calibration site near Chester, Arkansas. Three targets were deployed with the LIDAR instrument. As previously mentioned, the targets were used to locate control points within the point cloud, to tie the scans together, and to tie the scans to geographical coordinates. The LIDAR data acquisitions were performed during good weather conditions because laser light scanners are more susceptible to atmosphere and weather effects (water molecules). The duration of each individual 360 degree scan lasted approximately 25 minutes.

### **2.3.3. RADAR**

GAMMA Remote Sensing recently developed and built a ground based portable RADAR interferometer referred to as a Gamma Portable RADAR Interferometer (GPRI-II). This portable RADAR, unlike previous terrestrial RADAR instruments from other manufactures, does not use aperture synthesis to obtain good azimuth resolution and is fully mobile. The instrument utilizes real-aperture antennas, with two emitter antennas and one receiver antenna (Figure 2.7), operating at a frequency of 17.2 GHz (Werner, 2008). The relatively high frequency utilized by this device allows the user to obtain high azimuth resolution (1m) and sensitivity to motion (<1cm). Minimal deployment effort was required and individual measurements were obtained in less than 36 seconds, with a field of view of 360 degrees and an operational distance of 0.1 to 4 kilometers (GAMMA Remote Sensing, 2011).



**Figure 2.7. GPRI-II features (from GAMMA Remote Sensing AG, 2011).**

The Southbound viewpoint at the calibration site was located approximately 15 feet West of the Southbound shoulder of I-540. This location allowed for collection of RADAR data with a short field of view (i.e. the RADAR was close to the sliding mass [approximately 100 feet]). The RADAR benchmark was placed due West of the center of the main scarp (in the direction of movement). Four concrete footings were utilized to deploy the GPRI-II at this viewpoint (Figure 2.8). Three concrete footings were used to secure the tripod legs to the ground using anchors, while the fourth concrete footing contained a survey monument that served to level the RADAR in the same position during each visit. The same RADAR setup was followed during each visit. Before acquiring images at the Southbound viewpoint, the GPRI-II was aligned to the 4<sup>th</sup> fence post (located to the West of the observation point and marked with surveying flagging) using the scope of the RADAR.

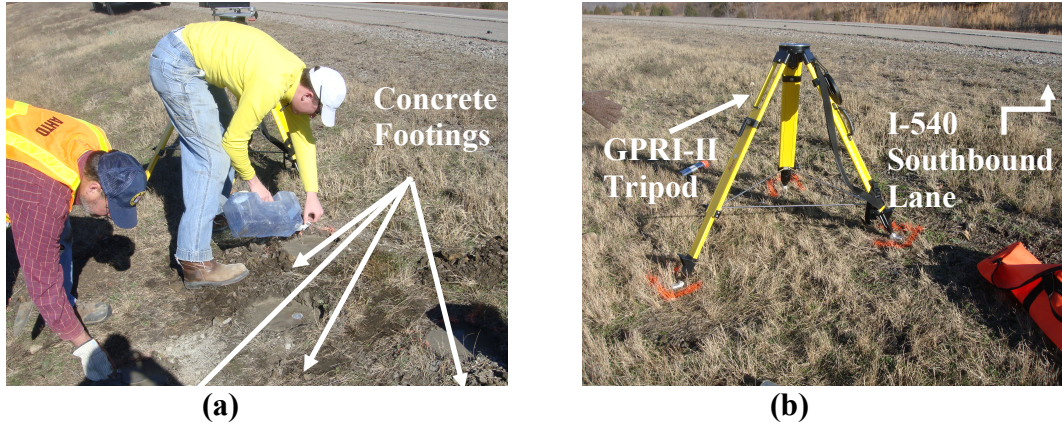


**Figure 2.8. a) Placing concrete footings for GPRI-II at the Southbound viewpoint at the calibration site, and b) tripod of GPRI-II anchored at the Southbound viewpoint near Chester, Arkansas..**

#### **2.3.4. Limit Equilibrium Slope Stability Analyses**

Using the data collected during a previously conducted AHTD geotechnical investigation and the UARK topographic survey, a limit equilibrium slope stability model was developed in SLIDE v. 5.044 (2010). Blow count data were the only available strength data that were obtained from the geotechnical investigation; therefore, a correlation (**Equation 2.1**) between corrected blow count ( $N_{60}$ ) and undrained shear strength ( $c_u$ ) was utilized to obtain undrained shear strength estimates. These estimates were input into the slope stability model.

$$c_u (psf) = \left( \frac{N_{60}}{30} \right) * 2000 \quad \text{Ritchy (1999)} \quad \text{Equation 2.1}$$

An elevation cross-section developed from the Autocad Civil 3D model was used to determine the slope surface geometry. Because the depths to each stratum were referenced to the ground surface, the inclinations of the stratum were also determined using the developed cross-section.

#### **2.4. Results Obtained from the Calibration Site**

The results obtained using the aforementioned three data acquisition methods (traditional, LIDAR, RADAR) at the calibration site are discussed in this section. The results obtained from

the total station measurements are described in Section 2.4.1. The results obtained from LIDAR measurements are presented in Section 2.4.2. The results obtained from the RADAR measurements are presented in Section 2.4.3. Finally, the results obtained from the limit equilibrium slope stability analyses are discussed in Section 2.4.4.

#### ***2.4.1. Total Station***

Site visits to the calibration site, subsequent to the installation of the 29 survey monuments (11/24/2010), were referred to as checks. A total of 17 checks were conducted to the calibration site near Chester, Arkansas. The total station device was used to monitor the displacement of each of the 29 survey monuments. The checks were performed during a 15-month period from November 2010 (Check 1) to February 2012 (Check 17). The total station measured displacements and elevation changes of each of the individual survey monument that were installed. Displacements to the West represented downhill movements.

Larger displacement values (in both the horizontal and vertical directions) were observed on and after May 2011 (Check 9) corresponding to the large amounts of precipitation experienced during the months of April and May of 2011. The precipitation and runoff saturated the soil in the slope, and the increased hydrostatic pore pressures led to a reduction in effective stress and induced/accelerated the displacement of the moving mass. The precipitation data for the 15 month period between October, 2010 and January, 2012 obtained from the National Oceanic & Atmospheric Administration (2012) is summarized in Table 1. The maximum horizontal displacements and maximum elevation differences observed using the total station for each of the site visits were plotted with the precipitation data. The horizontal displacements and elevation differences are plotted as a function of time including precipitation data (Figure 2.9 and Figure 2.10, respectively).

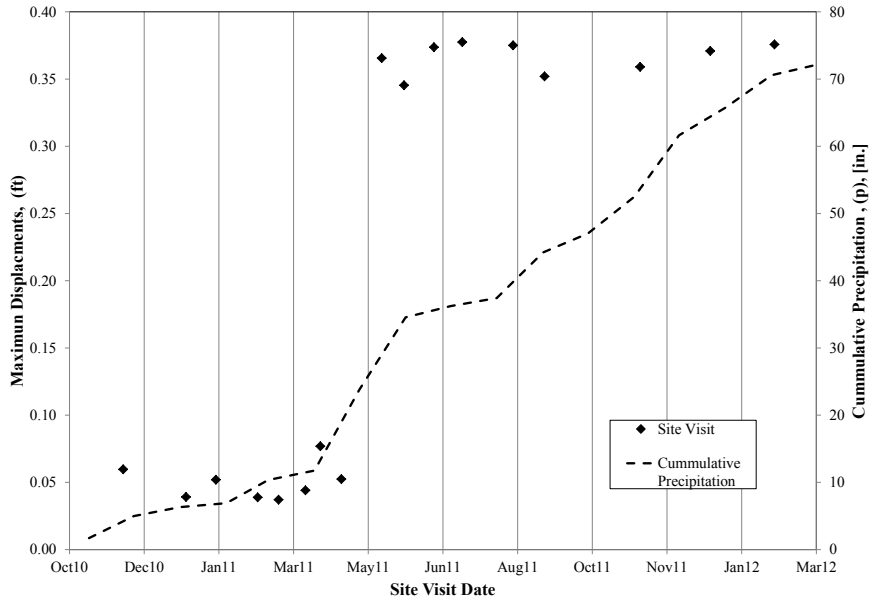


**Figure 2.9. Horizontal displacements measured and precipitation data for calibration site.**

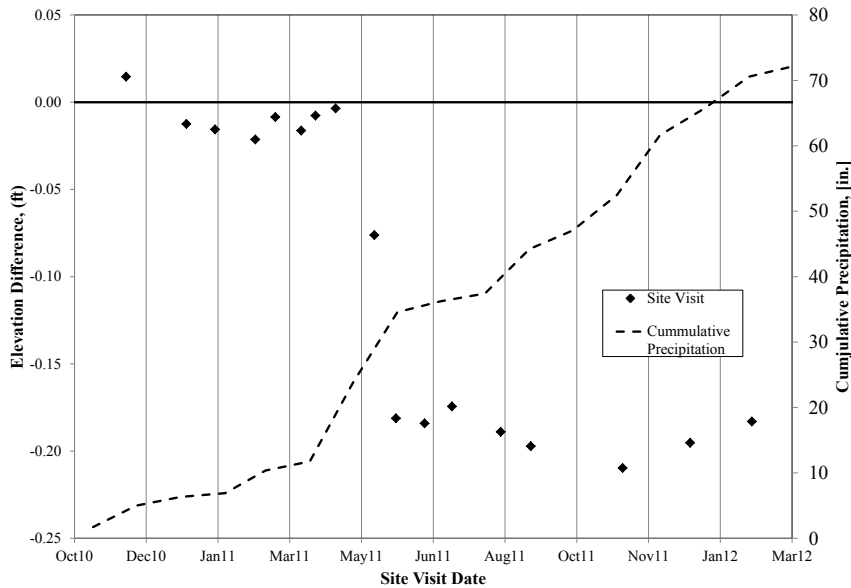


**Figure 2.10. Elevation differences measured and precipitation data for calibration site.**

Three distinct displacement areas were delineated to characterize the moving mass (Figure 2.11). The red zone was the area where the largest horizontal displacements were observed; the monuments bounded by orange zone had moderate horizontal displacements. Large amounts of movement of the survey monuments were expected to occur in the area below

the main scarp which is in agreement with the observed movements. The yellow zones were established where the monuments experience zero displacement or low displacements values.

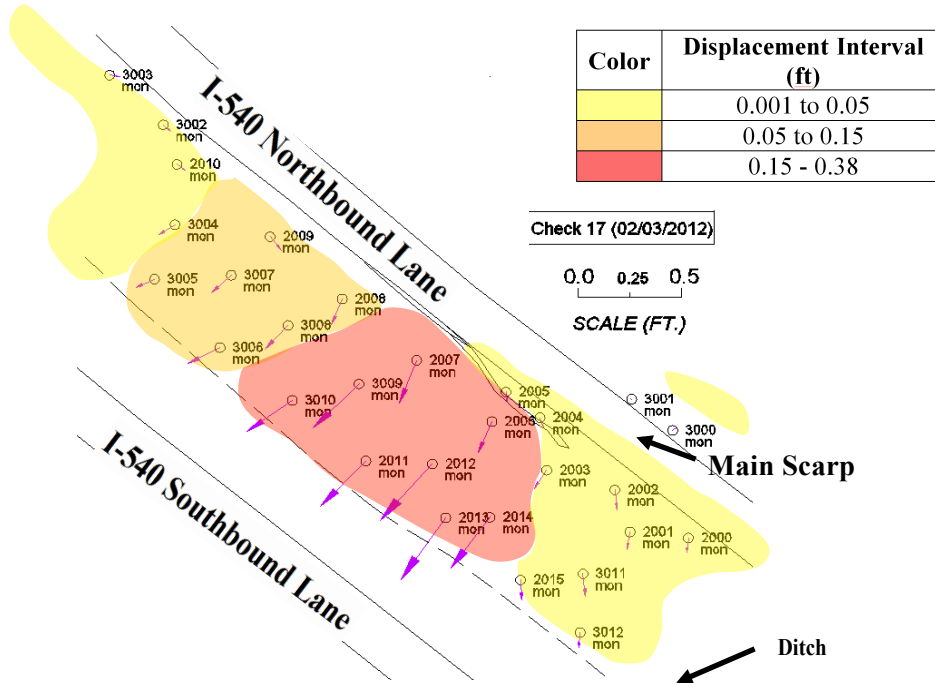


**Figure 2.11. Displacement areas for the calibration site; different colors represent the different displacement intervals [in color].**

Similarly, four distinct zones were delineated to characterize the vertical movement of the slide after analyzing the elevation differences measured on each survey monument during the checks. Vertical displacements were grouped in different intervals depending of the amount and direction of movement that was experienced. A rotational behavior was observed in the landslide at the calibration site. Downward movements were observed in the survey monuments installed at the head area of the slide and uplift movements were measured in the monuments installed at the toe area of the slide. A schematic illustrating the four different sections of elevation difference is presented in Figure 2.12.

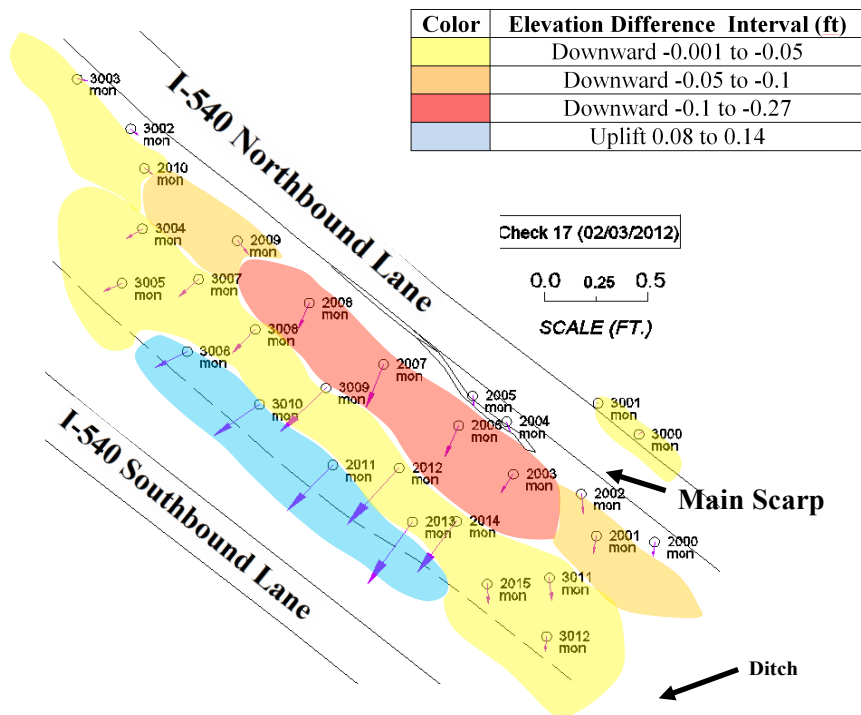


**Figure 2.12. Zones of vertical movements for the calibration site; red zone represents largest down movements, orange zone represents down medium movements, yellow areas low to zero down movement, and blue areas represent uplift movement [in color].**

Although the total station data was useful in monitoring the horizontal displacement of the slope, the limited spatial resolution prevented the identification of the exact extents of the sliding surface and the magnitude of the vertical deformation. As discussed in the next section, the surfaces created from the LIDAR data are more refined and are therefore more conducive to monitoring the extents of the head scarp and the vertical deformation of the slope.

#### **2.4.2. LIDAR**

Negative (downward) displacements were detected in the Southbound lane of I-540. The downward movements observed in the I-540 Southbound lane were the result of the expansion and contraction of the concrete pavement. The main scarp location, as obtained using the LIDAR bare earth method, also matched the location obtained with the total station measurements. The volume surface obtained using the LIDAR bare earth correction method for the site visits

between March 17<sup>th</sup>, 2011, and June 6<sup>th</sup>, 2011, is presented in Figure 2.13a. Progressive movement of the main scarp from the May 17<sup>th</sup>, 2011, surface to the June 8<sup>th</sup>, 2011, surface are illustrated in Figure 2.13b.

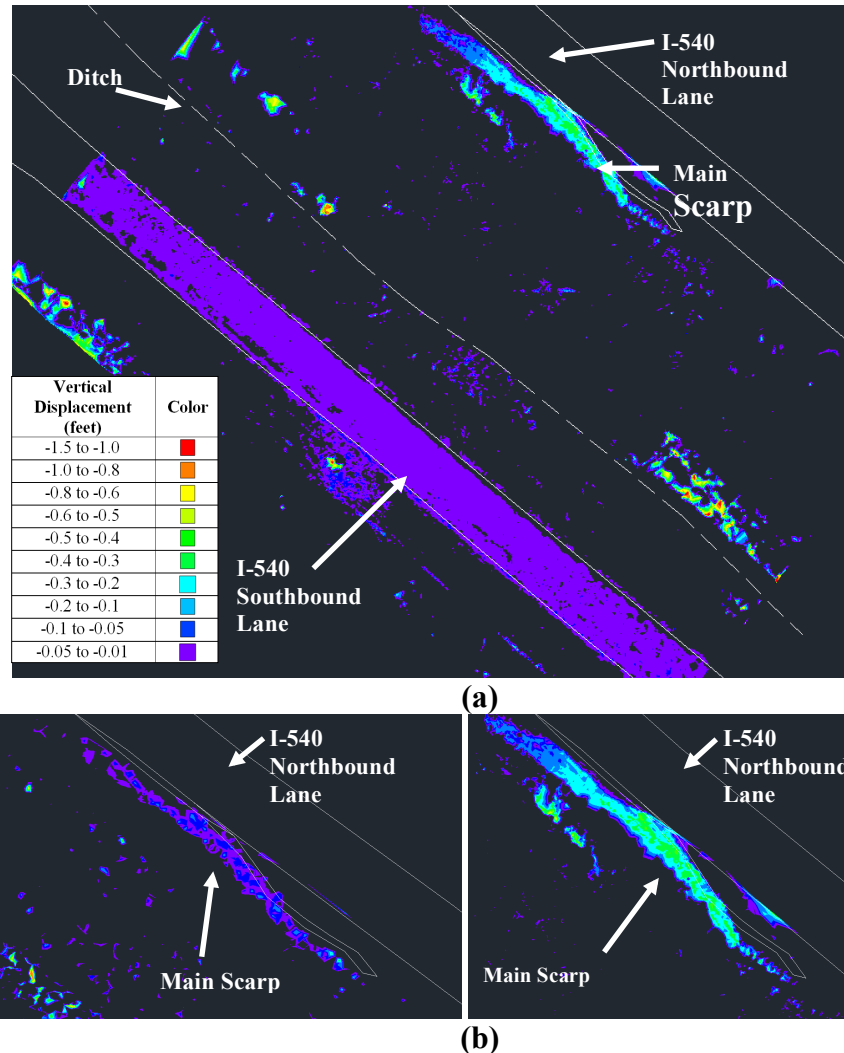


**Figure 2.13. a) Volume surface 03/17/11 to 06/08/11 (obtained using bare earth correction method) where maximum elevation difference on the main scarp was observed, and b) zoomed view to the main scarp where progressive movement was observed from 05/17/11 to 06/08/11 [in color].**

The three-dimensional (3D) surfaces generated from the LIDAR data was more refined than the 3D surface generated from the total station data because the point source sampling was much higher using LIDAR, as compared with the total station data. However, because the LIDAR does not observe the same points within each scan, the LIDAR point clouds can not be

used to monitor horizontal displacement of the slope. Although limited point data obtained from the total station, the data were observed with each scan, allowing for horizontal displacement monitoring of the slope, as shown previously in Figure 2.11.

### 2.4.3. RADAR

Radar images obtained using the 250ms chirp permitted a closer and better interpretation of the site than longer chirp lengths. In fact, due to the RADAR data acquisition proximity to the site; a lower chirp would have produced better MLI images, but the system only allowed for 250ms to be the lowest chirp possible. The I-540 Northbound lane, the I-540 Southbound lane, the ditch, and the terrain located to the East of the I-540 Northbound lane are appreciated in the produced MLI images. Some saturation is observed in the images due to the traffic of vehicles traveling along the I-540 lanes. The MLI data, as obtained after the initial processing of the RADAR (GPRI-II) data for the calibration site using the 250ms chirp, are presented in polar and rectangular coordinates in Figure 2.14.

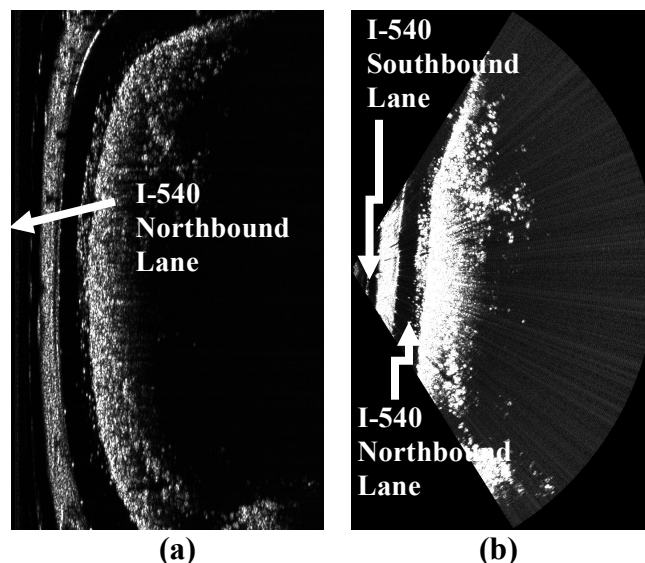


**Figure 2.14. a) MLI RADAR image obtained from southbound viewpoint in polar coordinates using 250ms chirp, and b) MLI RADAR image obtained from southbound viewpoint in rectangular coordinates using 250ms chirp.**

Interferograms were created for the different visits to the Southbound viewpoint in calibration site. The interferograms developed for the different visits to the Southbound viewpoint do not show a progressive movement of the landslide or main scarp with time. Vegetation was believed to be the major factor affecting the images for the interferograms. In the interferograms images, the green color represents zero movement and purple color represents movement values of 1.77cm. Two interferograms developed for the Southbound viewpoint, one with a time span of one month and a second with a time span of 11 months are presented in polar coordinates in Figure 2.15.

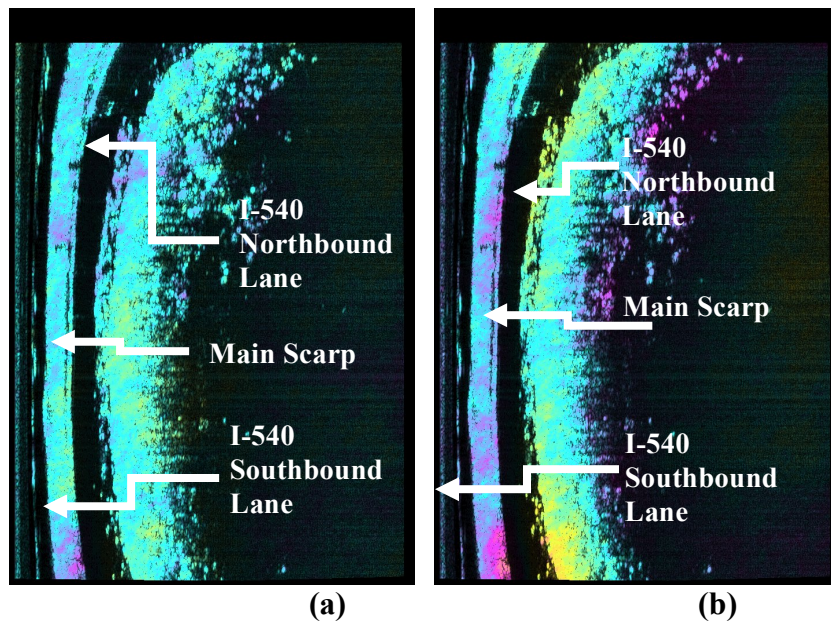


**Figure 2.15.** a) Southbound viewpoint interferogram from 03/08/11 to 03/26/11, and b) southbound viewpoint interferogram from 03/08/11 to 02/26/12.

#### ***2.4.4. Limit Equilibrium Slope Stability Analyses***

The parameters that were utilized within the slope stability analysis for the Chester slide are presented in Table 2.1. The obtained factors of safety against sliding are presented Table 2.2, and the results of the SLIDE v. 5.044 (2010) limit equilibrium slope stability analysis are displayed in Figure 2.16. A factor of safety of 0.999 was obtained from the analysis. Based on

this factor of safety, movement of the slope was anticipated. This back-analysis of the slope provided justification for the movement that was observed at the site.

**Table 2.1. Summary of soil parameters used in the slope stability analysis for calibration site**

Borehole	Depth (ft)	Description	N-Value	N <sub>60</sub>	Unit Weight (pcf)	Undrained Strength (S <sub>u</sub> ) (psf)	Undrained Strength (S <sub>u</sub> ) (psf)	Undrained Strength (S <sub>u</sub> ) (psf)
				CF=1.29		AHTD (125*N)	UARK (33*N)	Terzaghi (120*N)
B-1	0.0 - 9.5	Clay w/ Sand	9	12	90.0	1125.0	297.0	1080.0
B-1	9.5 - 32.0	Clay w/ Gravel	10	13	110.0	1250.0	330.0	1200.0
B-1	32.0 - 54.5	Shale	-	-	-			
B-3	0.0 - 24.0	Clay w/ Gravel	8	10	110.0	1000.0	264.0	960.0
B-3	24.0 - 45.0	Weathered Shale	23	30	115.0	2875.0	759.0	2760.0
B-3	45.0 - 62.0	Shale	-	-	-			
B-6	0.0 - 15.0	Clay w/ Gravel	13	17	110.0	1625.0	429.0	1560.0
B-6	15.0 - 26.0	Weathered Shale	30	39	115.0	3750.0	990.0	3600.0
B-6	26.0 - 44.0	Shale	-	-	-			

**Table 2.2. Summary of factors of safety obtained using different SPT-S<sub>u</sub> correlation methods for calibration site**

Correlation Method	Factor of Safety (FS)
UARK	1.003
Terzaghi	3.352
AHTD	3.384

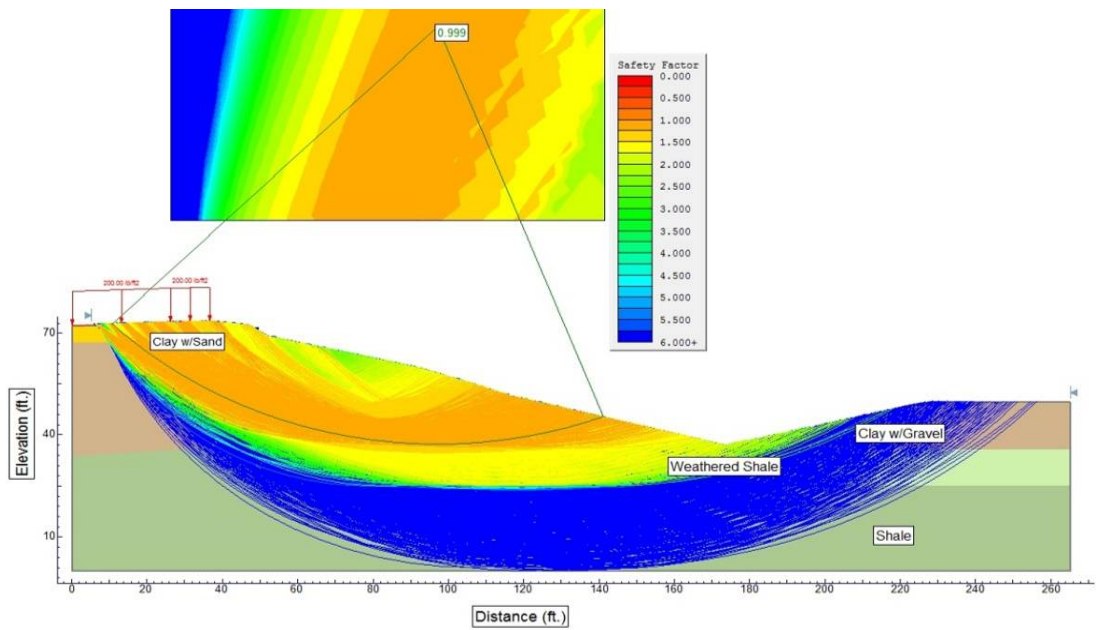


**Figure 2.16. Computed UARK slip surfaces using SLIDE 5.044 (2010).**

## **Chapter 3. Validation Site Near Malvern, Arkansas**

### ***3.1. Introduction***

At the validation site located near Malvern, Arkansas (Figure 3.1), the sliding mass extended under Interstate 30, under Highway 84 (located to the North of Interstate-30), and under Haltom Road (located to the South of Interstate-30). The zone of earth movement, at the validation site, was approximately 1100 feet wide (oriented parallel to the roadway). The continuing movement (lateral and downward) of the slide required frequent maintenance to re-level and patch the displacement that developed across the lanes. The potential negative impacts from this slope failure are significantly greater than those at the calibration site due to the size of the slide at the validation site and the quantity of traffic on Interstate-30. Because of the amount of movement at this site, since the completion of construction, a documented history exists for this site.

### ***3.2. Validation Site Overview***

Although the landslide at this site had previously unknown extents, the effects of the landslide were noticeable. The site is composed of private land on a hillside, a two lane highway (Highway 84), a median between Highway 84 and the interstate (Interstate 30), a median between the Westbound and Eastbound lanes of I-30, a median between I-30 and Haltom Road, Haltom Road, and a strip of vegetation between Haltom Road and the Ouachita River. The Ouachita River is believed to contribute to the instability of the site by removing the toe of the landslide and adding changes in the pore water pressure. Photographs of the site, taken by UofA personnel during the site visit in December 2010, are presented in Figure 3.2.



**Figure 3.1. Location of project site located at Log Mile 95.7 on Interstate 30 near Malvern, Arkansas. Anticipated slide area is shaded in red (Google Maps, 2011).**



**(a)**



**(b)**

**Figure 3.2. a) Looking Southwest from the hillside between Highway 84 and I-30, and b) looking west towards I-30 at the validation site near Malvern, Arkansas in December 2010.**

### ***3.3. Data Acquisition, Geotechnical Exploration and Limit Equilibrium at the Validation Site***

Three remote sensing methods were also utilized to acquire data at the validation site. The three methods consisted of total station, LIDAR, and RADAR. Each of the methods are discussed in the subsequent sections. Furthermore, the procedures utilized to collect data collected during the geotechnical investigation and the slope stability analyses are presented.

### 3.3.1. Total Station

The Malvern site was instrumented with 53 survey monuments using the same procedures that were used at the Chester site (as previously described for calibration site). Forty-one monuments were installed on December 3<sup>rd</sup>, 2010 and twelve monuments were installed on January 6<sup>th</sup>, 2011. The monuments (Figure 3.3) were installed in five lines (Figure 3.4) along the interstate (East-West direction). From North to South, the first line (6 monuments) was located north of the Highway 84; the next two lines were installed in a staggered (zigzag) pattern, and were located in the median between Highway 84 and the Westbound lane of I-30 (22 monuments); the next line (where the total station benchmark [Point 1000] was located) was in the median between the I-30 lanes (12 monuments); the fifth line was located just South of the I-30 Eastbound lane (12 monuments, these were the monuments installed on January 6<sup>th</sup>).



**Figure 3.3. a) Installation of survey monument in the ground by UofA and AHTD personnel, and b) survey monument installed in the ground using Quickcrete®.**

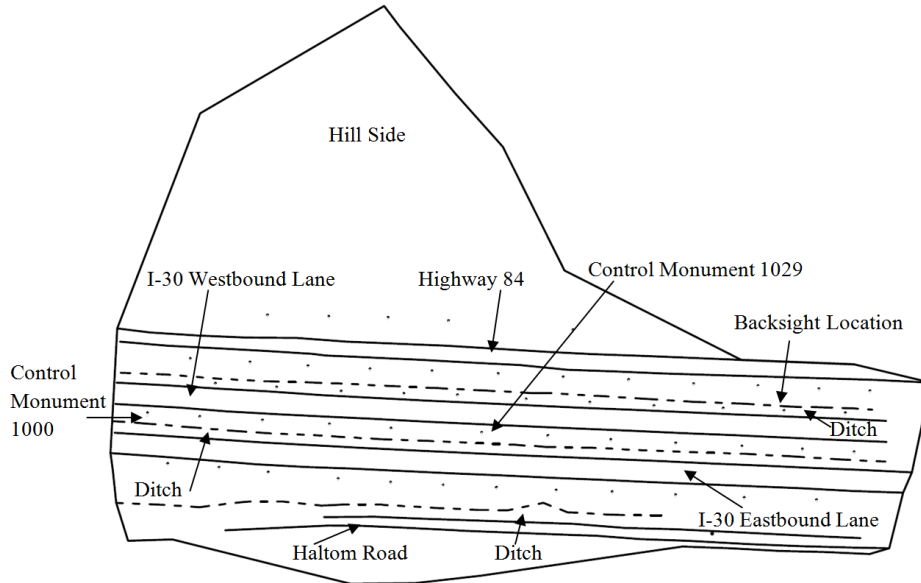


**Figure 3.4. Plan view of survey monument positions installed in validation site near Malvern, Arkansas.**

### **3.3.2. LIDAR**

At the Malvern site, two of four LIDAR occupation locations coincided with the RADAR acquisition locations (NE and SW viewpoints). Due to the range limitation of the LIDAR, three other locations were selected along the I-30 Westbound lane to capture the full extent of the sliding mass. The LIDAR data were obtained by AHTD personnel using the same methodology that was applied for the validation site. At each observation point, scans (360 degrees) were collected. Collecting LIDAR point clouds consisted of acquiring the coordinates and intensity ( $x, y, z, i$ ) of millions of points around each study area. As with the calibration site, targets were also positioned on known survey monuments along the site to link each scan to state coordinates during the data reduction process.

### **3.3.3. RADAR**

As previously mentioned, and in a similar manner to the procedures utilized at the calibration site, the RADAR observations were acquired from two locations. However, unlike with the calibration site where one of the two positions was located a large distance away from

the site, both of the RADAR acquisition positions at the validation site were located within the site. One of the positions was located South of the traveled lanes (in Halton Road) and the other position was located to the North of the traveled lanes (in between the I-30 Westbound lane and Highway 84).

#### ***3.3.4. Geotechnical Exploration***

Alternating Shelby Tube (ST) and Standard Penetration Test (SPT) samples were collected on alternating 5 foot intervals to a depth of 65 feet. Continuous ST sampling was conducted from a depth of 65 feet to a depth of 75 feet below the ground surface. This sampling program was intended to allow for sampling of the material at the sliding interface (as identified previously from inclinometers data collected at the site [Westerman, 2006]). After 75 feet the sampling procedure consisted of alternating ST and SPT every 5 feet. When a Shelby tube could not be pushed or became bent, a SPT test was conducted; rock coring was then conducted until the final depth of the borehole. Due to time constraints and safety concerns, Borehole B-5 (Figure 3.5) located in the median of I-30 was canceled, and was not drilled.

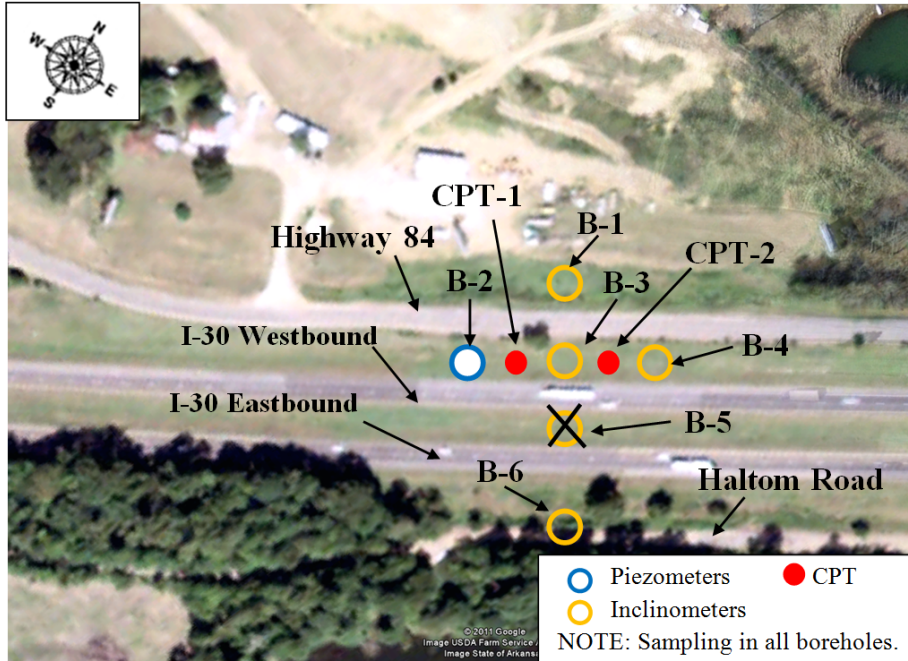


**Figure 3.5. Geotechnical investigation borehole locations at the validation site (modified from Google Maps, 2011).**

Four inclinometers and one vibrating wire piezometer were installed at the validation site in Malvern, Arkansas. The in-situ instrumentation was installed during the first two weeks of October, 2011. The inclinometers and vibrating wire piezometer were installed by AHTD personnel under the direct supervision of UofA personnel. A nested vibrating piezometer was installed in Borehole B-2 to determine the pore water pressure fluctuation as a function of time. The nested piezometer consists of five vibrating wire sensors at different depths. The transducers were placed at the following depths: 16, 37, 58, 79, and 100 feet.

### ***3.3.5. Limit Equilibrium Slope Stability Analyses***

Using the data collected during a previously conducted AHTD geotechnical investigation and the UARK topographic survey data, a limit equilibrium slope stability model was developed in SLIDE v. 5.044 (2010). Like with the calibration site, blow count data were the only available strength data from the geotechnical investigation; therefore, the Ritchy (1999) correlation was utilized.

After performing the initial slope stability analyses, the results obtained from the aforementioned geotechnical exploration were also utilized to perform additional slope stability analyses. An elevation cross-section developed from the Autocad Civil 3D model was used to determine the slope surface geometry. Because the depths to each stratum were referenced to the ground surface, the inclinations of the stratum were also determined using the developed cross-section.

### ***3.4. Results Obtained from the Validation Site***

The results obtained 1) using the aforementioned three remote sensing data acquisition methods, 2) from the geotechnical exploration, and 3) from the slope stability analyses that were conducted for the validation site are discussed in this section. The results obtained from the total station are described in Section 3.4.1. The results obtained from LIDAR are presented in Section 3.4.2. The results obtained from the RADAR are presented in Section 3.4.3. The results obtained from the geotechnical exploration are discussed in Section 3.4.4, and the results obtained from the slope stability analyses are presented in Section 3.4.5.

#### ***3.4.1. Total Station***

The total station results that were obtained at the validation site were inconclusive because of the location of the observation point and backsight point. Specifically, the points were located parallel with direction of movement (moving with the slope) instead of perpendicular to the direction of movement (slope moving toward the points). Therefore, the amount of movement was more of a function of the turning angle than electronic distance measurement, which resulted in errors in the measurements.

#### ***3.4.2. LIDAR***

Four LIDAR scans (per date) were required to cover the extent of the slide area at the validation site. Even though, the different scans for each site visit were registered and unified,

the movement of the landslide located at the validation site was not fully detected using LIDAR. Specifically, the size, complexity, and topography of the site prevented detection of the moving mass. The variability in the sensor setup may have introduced some noise into the final images. After analyzing the data from the monitoring devices utilized at the validation site it was concluded that the four LIDAR scans locations were inside the moving mass. Therefore, the LIDAR movements obtained were not relative to a fixed point, resulting in the poor correlation that was observed. The progressive downward elevation difference of the validation site in a time span of six months is shown in Figure 3.6.

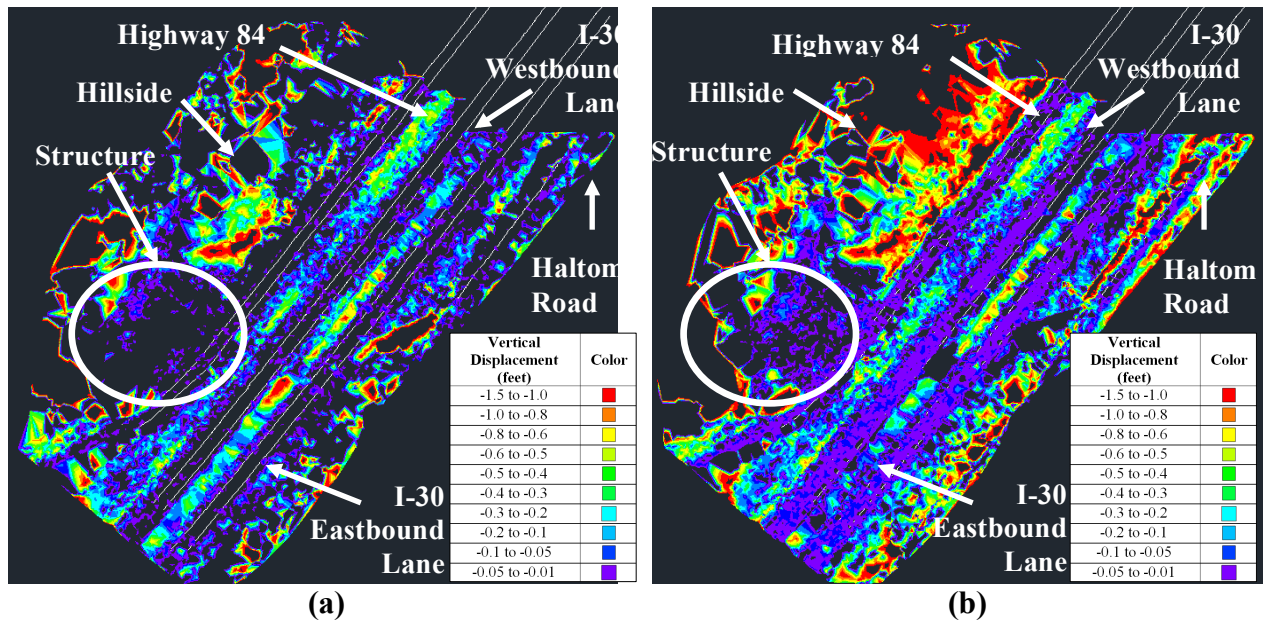


Figure 3.6. a) Volume surface (062711-080111) using bare earth correction method, and b) volume surface (062711-120211) using bare earth correction method [in color].

### 3.4.3. RADAR

Like the inconclusive total station and LIDAR results, the RADAR results were also inconclusive. The RADAR results that were obtained at the validation site were inconclusive because of the location of the observation points. Specifically, because of the topography and surrounding vegetation (trees) both of the observation the points were located within the sliding

mass. Therefore, to acquire images that contained the whole site, the RADAR images were acquired with a high chirp rate when they should have been acquired with a low chirp rate to enable visualization of the movement. In summary, although this site was selected as the validation site, it was not a good site for validation because of the limited vantage points (leading to inconclusive results from all of the remote sensing methods).

#### ***3.4.4. Geotechnical Exploration***

The results obtained from the in-situ instrumentation and laboratory testing that were installed and performed in association with the geotechnical exploration are presented in this section. Specifically, the inclinometer data, the vibrating wire data, and the laboratory testing data are presented. More detailed information about the geotechnical exploration can be found in Conte (2012).

##### ***3.4.4.1. Inclinometers***

The inclinometers installed within the validation site were used to generate two different cross-sections. Inclinometers installed within Boreholes B-1, B-3, and B-6 formed a North-South cross-section; whereas inclinometers within Boreholes B-3 and B-4 formed an East-West cross-section. The data obtained from the inclinometers installed at the validation site is summarized in Table 3.1. The slope inclinometers allowed for the observation and measurement of ground movement at different depths at the validation site. The sliding surface was interpolated from the three inclinometers located within Boreholes B-1, B-3 and B-6 (Figure 3.7 and Figure 3.8). The inclinometer data coupled with the site stratigraphy observed during the subsurface investigation (Figure 3.9 and Figure 3.10) indicate that the failure surface was located within the limestone-weathered shale layer.

**Table 3.1. Summary of results for inclinometers installed at validation site.**

Inclinometer	Depth to Slip Plane	Date	Incremental Displacement	Days	Displacement Rates		Average
	ft.		inch		inch/day	inch/year	
B-1	51.5	Nov. 8	0.0066	26	0.0003	0.093	0.13
		Dec. 20	0.0189	68	0.0003	0.101	
		Feb. 10	0.0687	120	0.0006	0.209	
B-3	64	Nov. 8	0.0012	26	0.0000	0.017	0.18
		Dec. 20	0.0411	68	0.0006	0.221	
		Feb. 10	0.1029	120	0.0009	0.313	
B-4	60	Nov. 8	0.0042	26	0.0002	0.059	0.13
		Dec. 20	0.0246	68	0.0004	0.132	
		Feb. 10	0.0687	120	0.0006	0.209	
B-6	60	Nov. 8	0.0021	26	0.0001	0.029	0.16
		Dec. 20	0.0333	68	0.0005	0.179	
		Feb. 10	0.0864	120	0.0007	0.263	

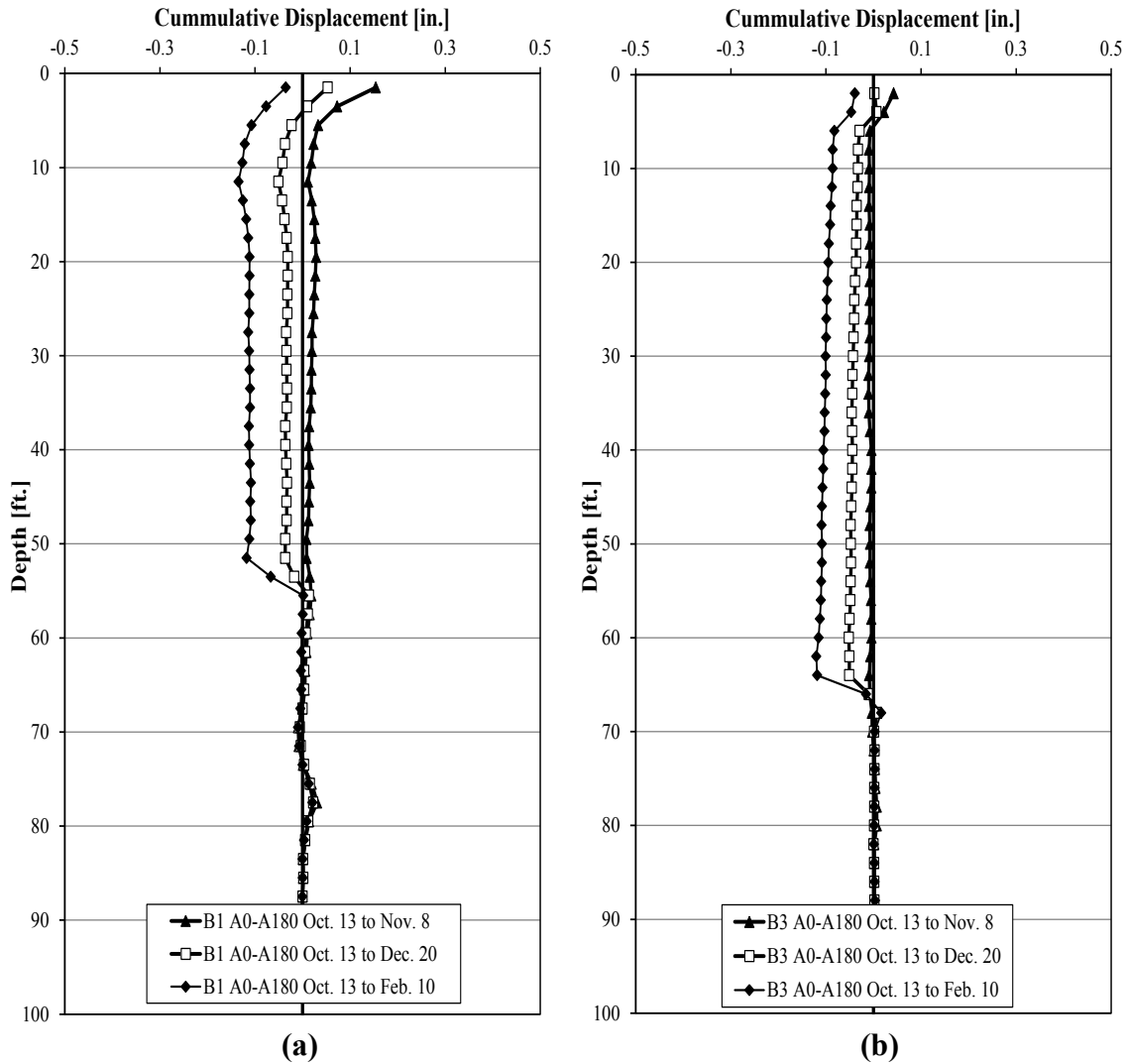


**Figure 3.7. Profile of the slope inclinometer installed at B-1 location for the site visits to the validation site, and b) Profile of the slope inclinometers casing installed at the B-3 location for the site visits to the validation site.**

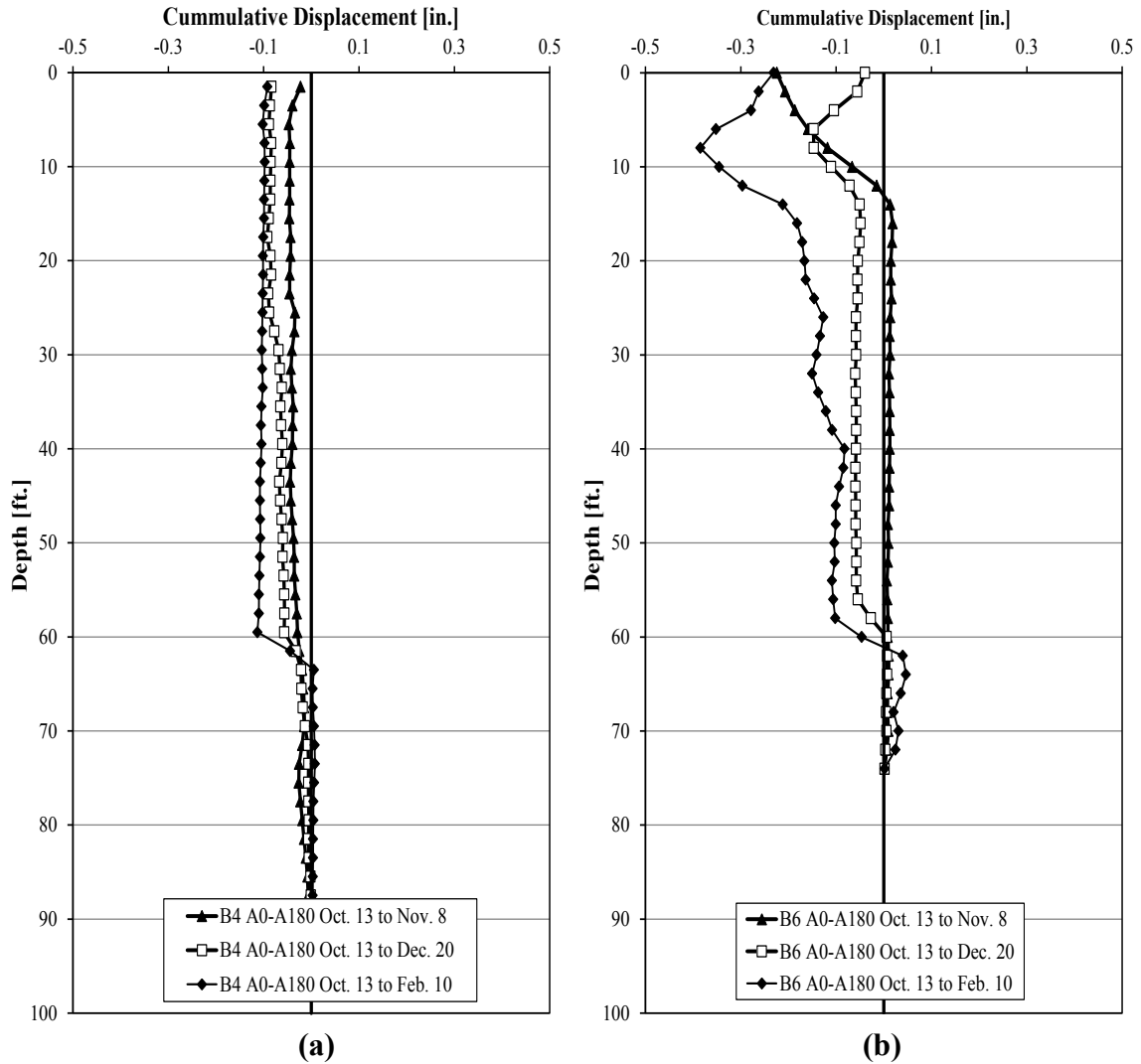


**Figure 3.8. Profile of the slope inclinometer installed at B-4 location for the site visits to the validation site, and b) Profile of the slope inclinometers casing installed at the B-6 location for the site visits to the validation site.**

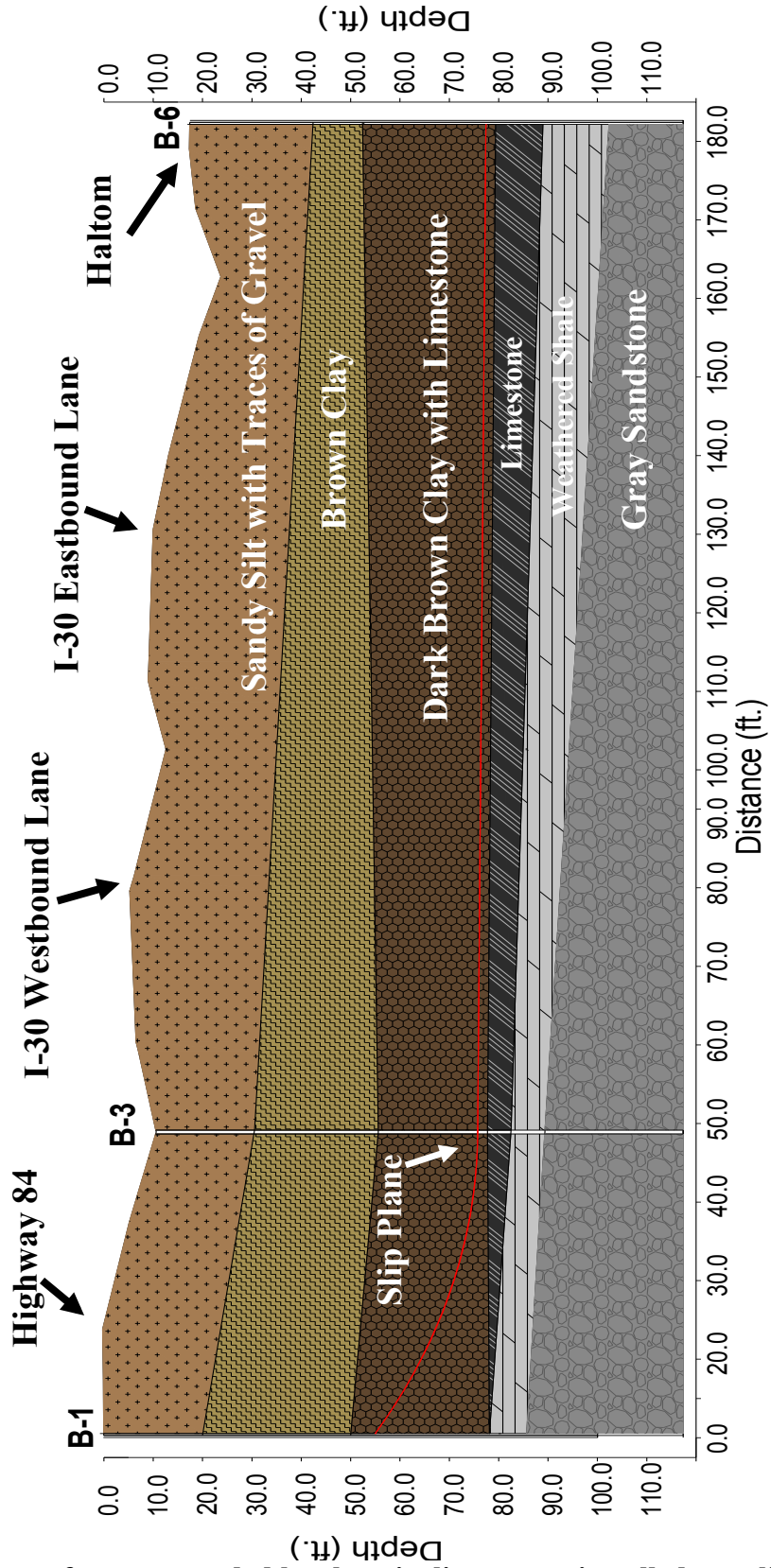


Figure 3.9. Sliding surface as recorded by slope inclinometers installed at validation site [in color].

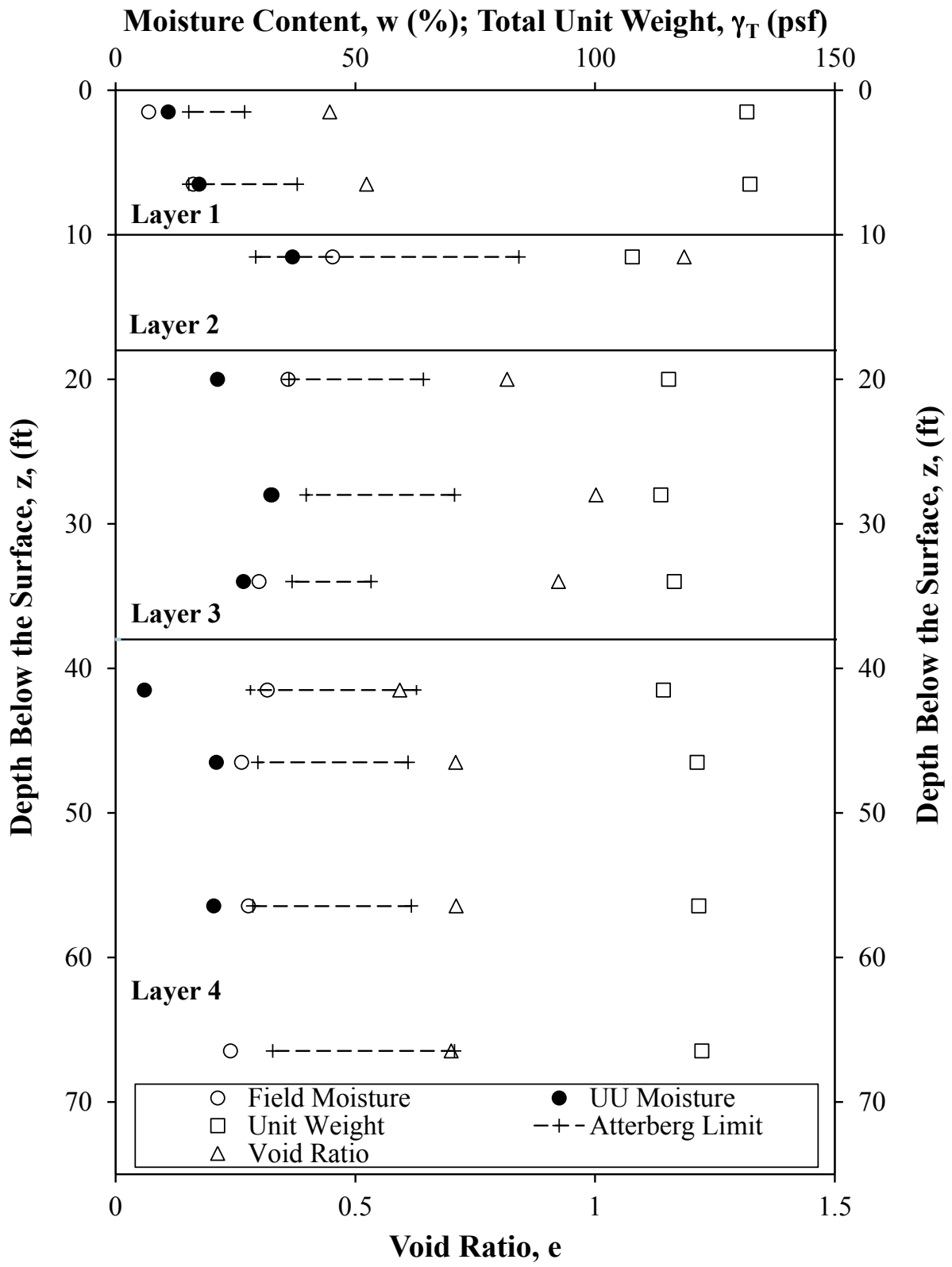
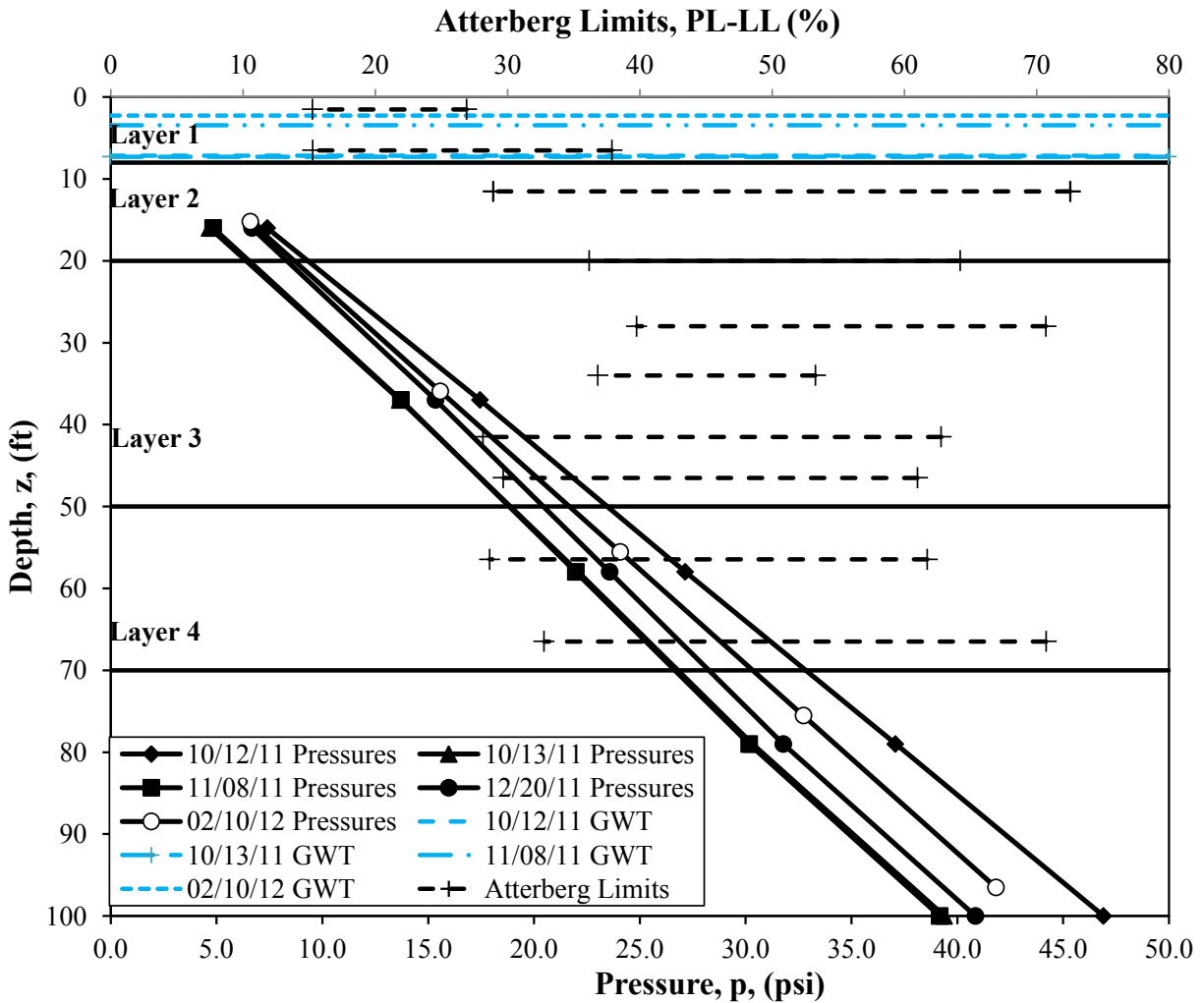


Figure 3.10. Design moisture content, unit weight and Atterberg Limits profile.

#### ***3.4.4.2. Vibrating Wire Piezometers***

The nested vibrating wire piezometer (VWP) was installed in Borehole B-2, in the median between Highway 84 and the Westbound lane of I-30. The vibrating wire piezometer was monitored over a four-month period between October 2011 and January 2012. Data was acquired during the last five site visits to the validation site.

Pressure changes at the location of the slip surface (as measured with the inclinometers) were not observed with the nested vibrating wire piezometer installed within Borehole B-2. However, artesian conditions could have affected the obtained measurements. The ground water table (GWT) depth was inferred from the pressures measured by the transducer sensors (installed at different depths) during the different visits. The GWT was consistent (except for the last site visit) at an approximate depth of 7.3 feet below the ground surface. The GWT depth measured with the nested vibrating wire piezometer coincided with the change in strata as indicated by a change in plastic index (PI) that was obtained from the subsurface investigation. During the last visit to the site, the calculated GWT was at a depth of approximately 2 feet below the ground surface (Figure 3.11). The increased elevation of the GWT correlated with, and was causative of, the increase in displacements rates measured by the inclinometers.



**Figure 3.11. Pressure obtained from the nested vibrating wire piezometer [in color].**

#### **3.4.4.3. Laboratory Results**

Unconsolidated Undrained triaxial (UU) tests were performed on the clay samples obtained from the Shelby tubes recovered at the validation site. The UU tests were performed in accordance with (ASTM D2850, 2007). A deviation from ASTM D2850 was that the measurement of the piston friction force at the beginning of the test was obtained by leaving a small gap between the piston and the top cap of the specimen. The results obtained from the strength investigation are presented in Figure 3.12.

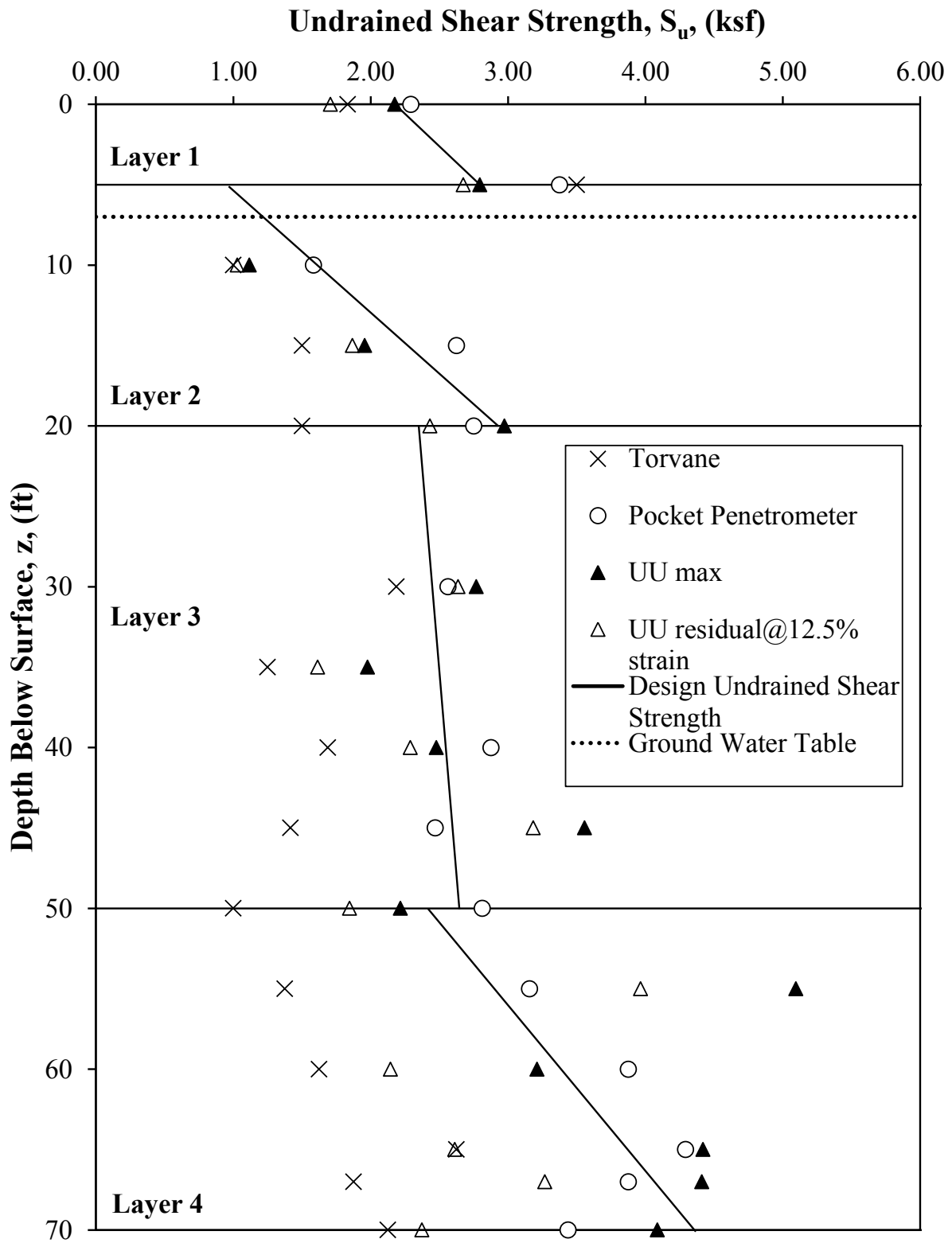


Figure 3.12. Design strength profile for validation site near Malvern, Arkansas.

Softening behavior was observed in all the specimens during UU testing. The maximum undrained shear strength values obtained varied with the depth of the sample, the moisture content and the soil type. Important parameters such as: the Peak Principal Stress Difference (PPSD), the peak maximum undrained shear stress ( $q$ ), the axial strain at PPSD, the axial strain at 50 percent PPSD, and the residual undrained shear stress at 12.5 percent axial strain were calculated for each test. A distinct loss of shear strength was observed to occur between the peak undrained shear stress values and the residual undrained shear stress values for most of the specimens recovered from depths greater than 61 feet below the ground surface. Normalized stress-strain curves were developed for each UU test. Normalized stress-strain graphs for the Boring B-2 specimens between 51.5 feet to 67.5 feet (the location of the anticipated sliding surface) are presented in Figure 3.13.

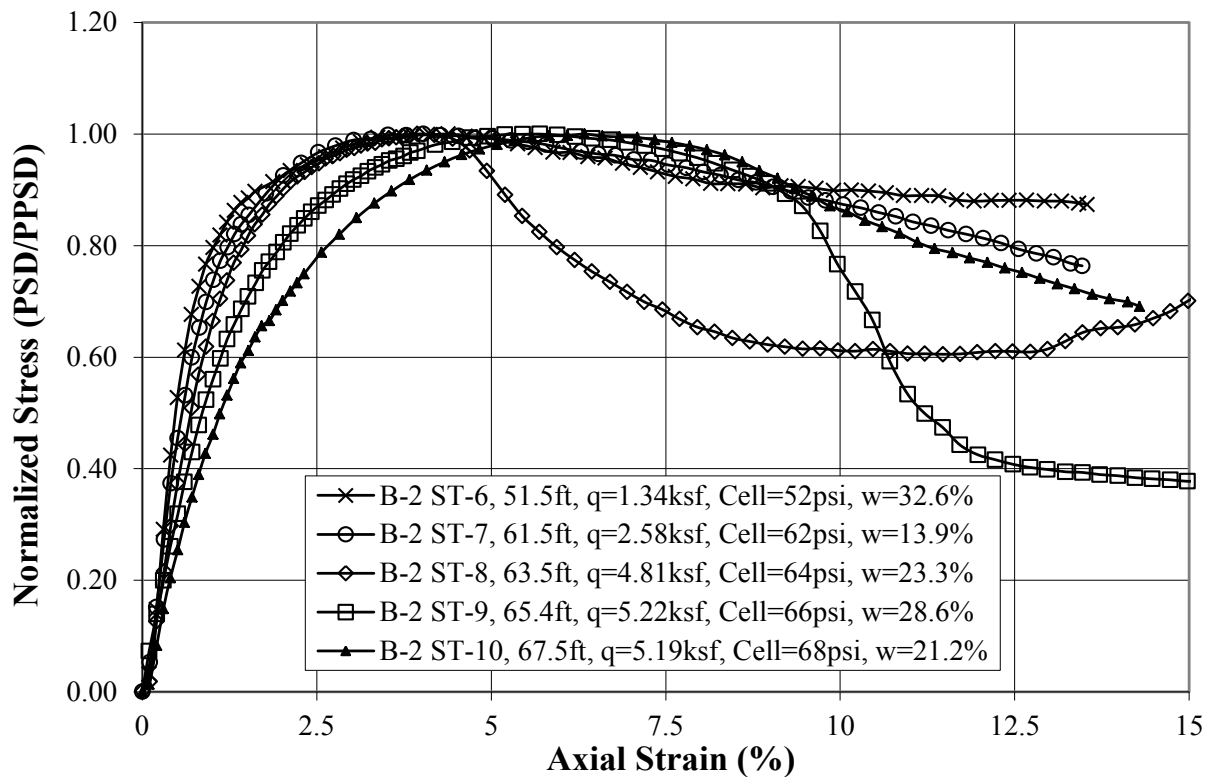


Figure 3.13. Normalized stress-strain graph of UU test results obtained from Boring B-2 specimens at validation site.

#### ***3.4.5. Limit Equilibrium Slope Stability Analyses***

The parameters that were utilized within the slope stability analysis for the Mavern slide are presented in

Table 3.2. The obtained factors of safety against sliding, as obtained from the initial slope stability analysis are presented in

Table 3.3, and the results from one of the SLIDE v. 5.044 (2010) preliminary limit equilibrium slope stability analyses, are displayed in Figure 3.14. Although a factor of safety of 0.999 was determined for the calibration site, a nonsensical factor of safety of 0.378 was obtained by using the same correlation as the calibration site at the validation site. Therefore, the aforementioned geotechnical investigation was performed to obtain new/refined soil parameters to utilize for additional slope stability analyses. Based on the analyses performed using the new/refined soil parameters (Table 3.4), the factor of safety that was obtained using the correlation that predicted the correct factor of safety at the calibration site (0.999) was still below unity at the validation site (0.679 as shown in Figure 3.15). Moreover, the factors of safety that were obtained by using the new/refined UU residual and UU max values were much higher than unity (Table 3.5 and Figure 3.16). Therefore, as previously mentioned, the pore water pressure must have been the cause for the initiation of sliding as opposed to the shear strength values. Or the shear strength parameters along a weakened zone, at the dark brown clay/limestone interface, were not identified or measured during the geotechnical investigation.

**Table 3.2. Summary of the initial soil parameters utilized in the initial slope stability analysis for the validation site.**

Borehole	Depth (ft)	Description	USCS Classification	N-Value	N <sub>60</sub>	Unit Weight (pcf)	Undrained Strength (Su) (psf)	Undrained Strength (Su) (psf)	Undrained Strength (Su) (psf)
							AHTD (125*N)	UARK (33*N)	Terzaghi (120*N)
INC1	0.0 - 23.5	Clay w/ Gravel	CL	12	16	90.0	1500.0	396.0	1440.0
INC1	23.5 - 54.5	Clay	CL	11	15	110.0	1375.0	363.0	1320.0
INC2	0.0 - 20.0	Silty Clay	CL	10	13	110.0	1250.0	330.0	1200.0
INC2	20.0 - 74.0	Clay	CL	15	20	115.0	1875.0	495.0	1800.0
INC2	74.0 - 81.0	Limestone	-	-	-	-	-	-	-

**Table 3.3. Summary of results for the preliminary slope stability analysis of the validation site.**

Correlation Method	Factor of Safety (FS)
Terzaghi	1.373
AHTD	1.430
UARK	0.378

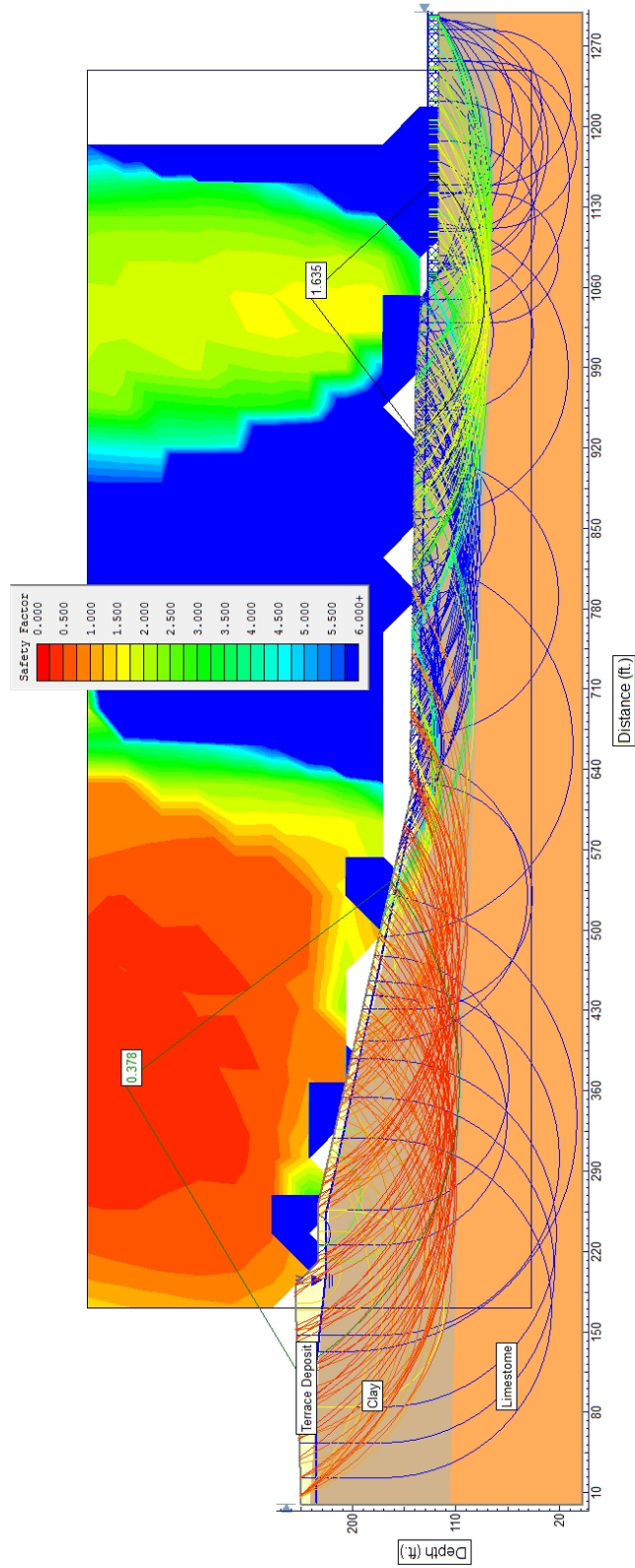


Figure 3.14. Preliminary slope stability model for validation site using UARK correlation.

**Table 3.4. Summary of the refined soil parameters used in the refined slope stability analysis at the validation site near Malvern, Arkansas.**

Borehole	Depth (ft)	Description	USCS Classification	N-Value	N <sub>60</sub> CF=1.32	SPT- Correlation Unit Weight (pcf)	Measured Unit Weight (pcf)	Undrained Strength (Su) (psf)		Residual Undrained Strength (Su) (psf)		
								UU Test	UU Test	UU Test	AHTD (125*N)	UARK (33*N)
B-1	0.0 - 20.0	Sandy Silt with Traces of Gravel	ML	12	16	105.0	114.45	1653.7	1532.27	1500.0	396.0	1440.0
B-1	20.0 - 50.0	Brown Clay	CL	19	25	110.0	112.48	2226.0	2107.16	2375.0	627.0	2280.0
B-1	50.0 - 80.0	Dark Brown Clay with Limestone	CL	23	30	120.0	116.77	3807.6	3052.74	2875.0	759.0	2760.0
B-1	80.0 - 100.0	Gray Sandstone	-	-	-	-	143.20			41679.6		
B-3	0.0 - 20.0	Sandy Silt with Traces of Gravel	ML	7	9	105.0	121.93	1803.8	1605.815	875.0	231.0	840.0
B-3	20.0 - 45.0	Brown Clay	CL	23	30	120.0	112.48	2226.0	2107.16	2875.0	759.0	2760.0
B-3	45.0 - 68.0	Dark Brown Clay with Limestone	CL	18	24	110.0	119.76	4201.6	3014.455	2250.0	594.0	2160.0
B-3	68.0 - 73.0	Limestone	-	-	-	-	158.75			196451.0		
B-3	73.0 - 77.0	Weathered Shale	-	-	-	-	129.21			11783.7		
B-3	77.0 - 100.0	Gray Sandstone	-	-	-	-	137.83			52607.1		
B-6	0.0 - 25.0	Sandy Silt with Traces of Gravel	ML	9	12	105.0	106.97	1503.6	1458.725	1125.0	297.0	1080.0
B-6	25.0 - 35.0	Brown Clay	CL	16	21	120.0	112.48	2226.0	2107.16	2000.0	528.0	1920.0
B-6	35.0 - 70.0	Dark Brown Clay with Limestone	CL	10	13	110.0	120.85	3150.4	2523.2325	1250.0	330.0	1200.0
B-6	70.0 - 72.0	Limestone	-	-	-	-	159.64			197849.2		
B-6	72.0 - 82.0	Weathered Shale	-	-	-	-	137.12			16781.3		
B-6	85.0 - 100.0	Gray Sandstone	-	-	-	-	148.52			93430.6		

NOTE: Shear strength for rock material determined by confined compression tests.

**Table 3.5. Summary of factors of safety obtained after refined slope stability analysis for the validation site.**

<b>Correlation Method</b>	<b>Factor of Safety (FS)</b>
UARK	0.679
Terzaghi	2.479
AHTD	2.674
UU TEST-residual	2.931
UU TEST-max	6.672

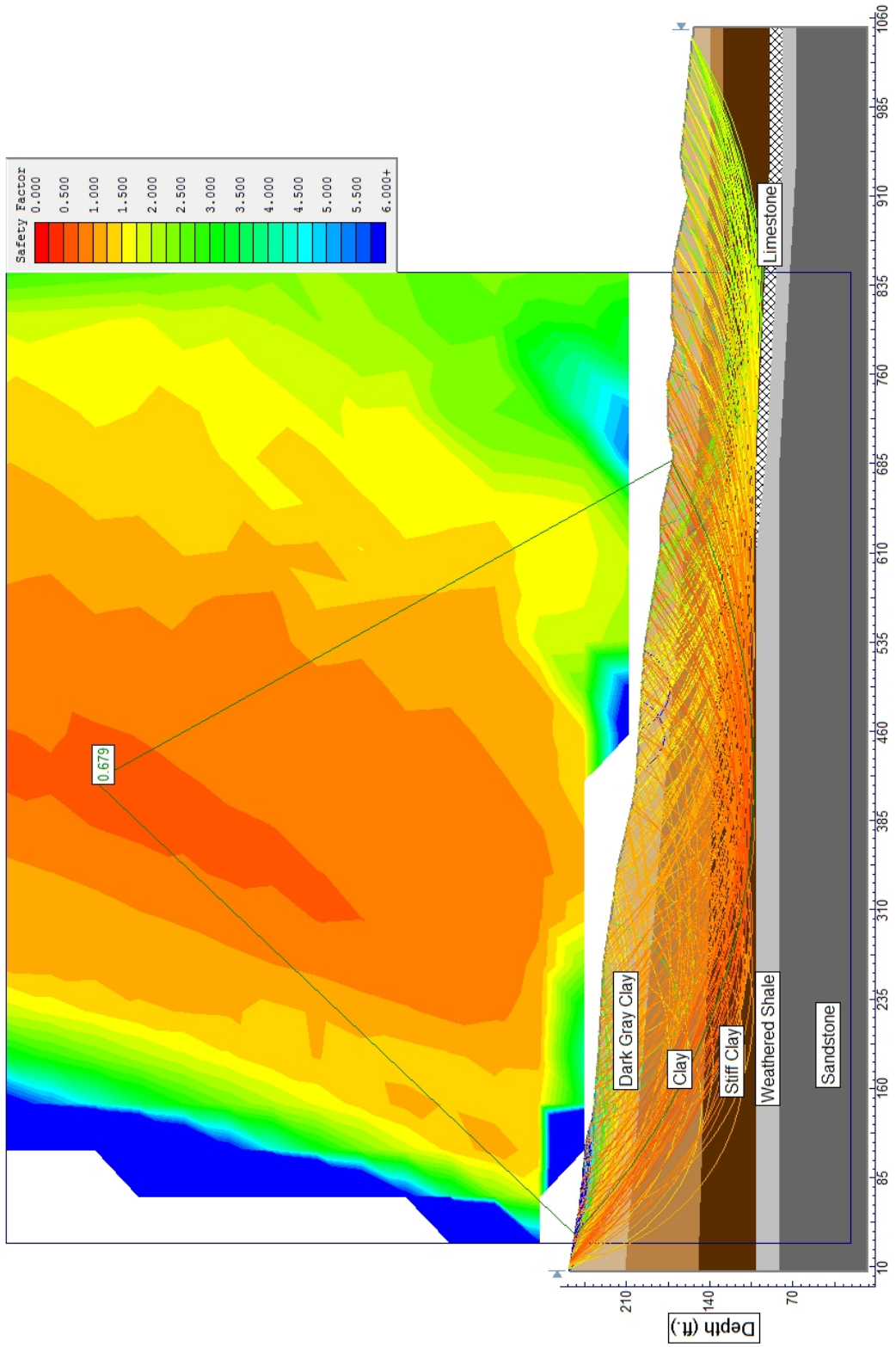
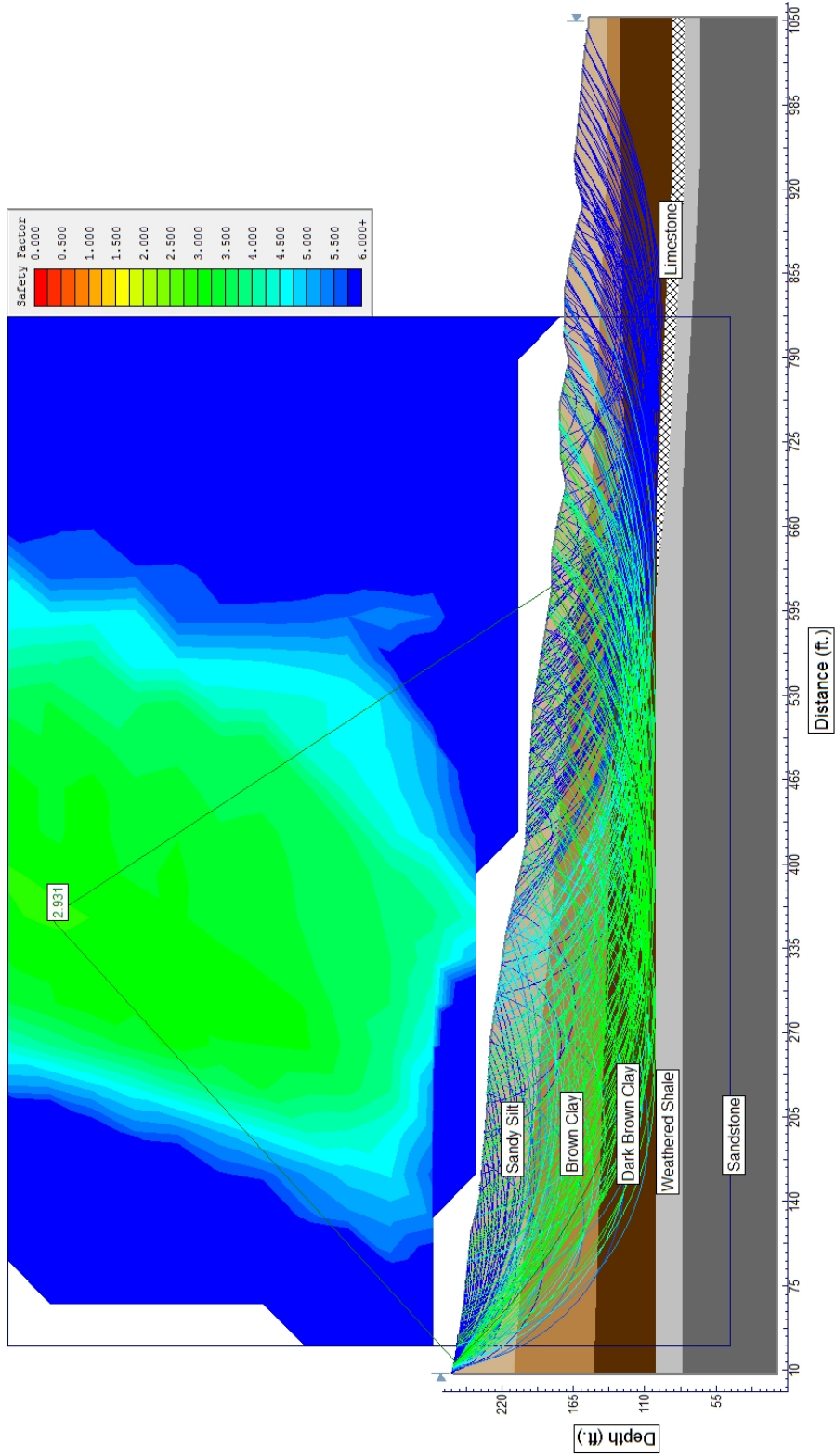


Figure 3.15. Refined slope stability model for validation site using UARK correlation.



**Figure 3.16. Refined slope stability model for validation site using UU test results (residual undrained strength).**

## **Chapter 4. Conclusions**

The three monitoring techniques (total station, LIDAR, RADAR) discussed in this final report may be used for landslide monitoring. Depending on the site specific features the use of one technique may be more advantageous than another. The total station was found to provide reliable results for monitoring relative small areas (up to 600 feet) where the amount of survey monuments required is not extensive. Conversely, when time and labor costs are of concern, LIDAR and RADAR systems may provide a better method to efficiently monitor large areas with a reduced investments in manpower and scheduling.

The total station data reduction process is less computationally and intellectually demanding than the more advanced remote sensing techniques (LIDAR and RADAR). Additionally, the total station data reduction can be performed in common datasheet programs without the usage of special software requirements. Although, the data processing of LIDAR and RADAR is more complex and data storage more intensive, automation of the data reduction procedures is possible. Also, the data collected using the LIDAR and RADAR may be visualized during the data acquisition process. This three-dimensional visualization of the data (LIDAR and RADAR) provides the opportunity for manual inspection and filtering of any erroneous data.

The location of the scanners during a remote sensing session is of vital importance to the obtained results. The scanner should be 1) placed downhill of the direction of anticipated movement and 2) the line-of-sight direction should be in the direction of movement. An elevated platform may be required for locations with limited viewpoints to meet these criteria.

## Chapter 5. References

- American Society for Testing and Materials, (2007), "Standard Methods for Uncosolidated-Undrained Triaxial Compression test on Cohesive Soils" Annual Book of ASTM Standards, Designation D2850, Vol. 4.09, ASTM, West Conshohocken, PA.
- Arkansas State Highway and Transportation Department (2010). "Geotechnical Report D04133," August 26.
- AutoCAD. Version E. 115.0.0. 2011. 2010 AutoDesk, Inc.
- Conte, Omar. (2012), "Slope Stability Monitoring Using Remote Sensing Techniques". Master of Science Thesis. University of Arkansas, May.
- Conte, O., and Coffman, R., (2012), "Slope Stability Monitoring Using Remote Sensing Techniques," ASCE GeoCongress 2012, Oakland, California.
- GAMMA Remote Sensing AG, (2011) "GAMMA Portable RADAR Interferometer II (GPRI-II) User Manual," Worbstrasse 225 CH-3073 Guemligen, Switzerland, February.
- Google Maps Website, (viewed August 2011), <http://maps.google.com/>.
- Griffiths, J., Stokes, M., and Thomas, R., (1999), "Landslides," Taylor & Francis, 1<sup>st</sup> Edition.
- Leica Cyclone (2010), Version 7.1.1 Documentation, Leica.
- National Oceanic and Atmospheric Administration Website (2012), "National Weather Service Forecast Office Tulsa, Oklahoma," website viewed March 16, 2012, <<http://www.nws.noaa.gov/climate/index.php?wfo=tsa>>.
- Nikon Instruction Manual, (2011), "Total station DTM-500 series," Nikon Corporation, Shinagawa-ku, Japan.
- Nikon Positioning Website, (2012), "Surveying Products," website viewed February 2, 2012, <[http://www.nikonpositioning.com/nivo\\_m.aspx](http://www.nikonpositioning.com/nivo_m.aspx)>.
- Slide (2010) Version 5.044 Documentation, Rocscience Inc.
- Werner, C., Strozzi, T., Wiesmann, A., and Wegmuller, U., (2008), "Gamma's Portable RADAR Interferometer," Proc., 13<sup>th</sup> FIG Symposium on Deformation Measurement and Analysis. Lisbon, May 12-15.
- Westerman, J., (2006) "I-30 Slide - Malvern: I-30 Section 21: Log Mile 95.7: Hot Spring County" Arkansas Highway and Transportation Department Memo to Robert Walters, February, 21 2006.

## Appendix A . LAStools©

Contained in this appendix are step-by-step procedures outlining the performing a bare earth correction method that was utilized to process the LIDAR data. These procedures were used to eliminate the vegetation points from the LIDAR point clouds. The ground points were used to create the volume surfaces. This step-by-step procedure starts after the point clouds have been exported from Cyclone as .pts file (Figure A.1). The procedure was performed using a batch file containing the following commands.

To convert the .pts file to .las file (Figure A.2) the command executed was:

```
txt2las.exe -i input_pts\slave_raw.pts -o output_las\slave_raw.las -iparse xyz -parse xyz  
lasinfo -i output_las\slave_raw.las -o output_reports\slave_raw.txt -histo classification 1
```

The file was then split in two file for a better workability with the computer resources. The command used was:

```
::split *_raw.las files into smaller files to reduce computational demand - MUST  
IDENTIFY NUMBER OF POINTS PRIOR TO THIS STEP  
lassplit -i output_las\slave_raw.las -o output_las\slave_spl.las -split 17000000
```

The command used to separate the vegetation points from the non-vegetative points in two different layers was the following:

```
lasground -i output_las\slave_spl.00000.las -o output_las\slave_cls00000.las -feet -  
elevation_feet -step 2 -spike 0.1  
lasground -i output_las\slave_spl.00001.las -o output_las\slave_cls00001.las -feet -  
elevation_feet -step 2 -spike 0.1
```

The result of the separation is illustrated in Figure A.3, Figure A.4 and Figure A.5.

The point cloud were then reduce for export to AutoCAD Civil 3D software, were the surfaces were created (Figure A.6). The command use was:

```
lasthin -i output_las\slave_cls00000.las -o output_las\slave_thn00000.las -  
keep_classification 2 -step 3 -lowest  
lasthin -i output_las\slave_cls00001.las -o output_las\slave_thn00001.las -  
keep_classification 2 -step 3 -lowest
```

Finally the file were merged back again to a single file using the following command.

```
lasmerge -i output_las\slave_thn00000.las output_las\slave_thn00001.las -o  
output_las\slave_thn.las  
lasinfo -i output_las\slave_thn.las -o output_reports\slave_thn.txt -histo classification 1
```

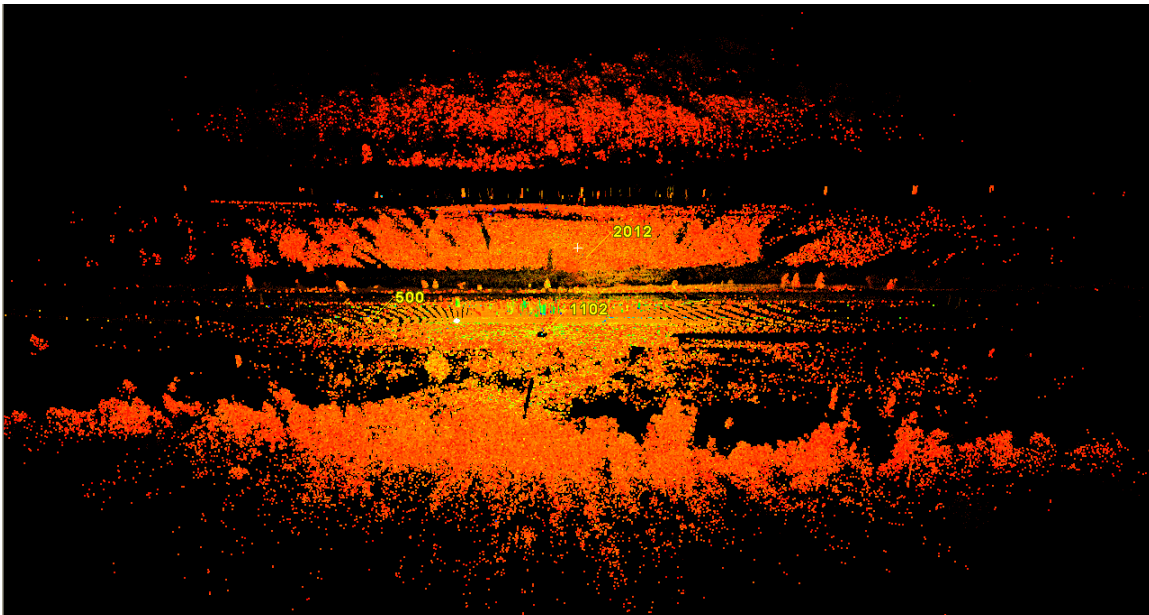


**Figure A.1. Point cloud for Chester site in Leica Geosystems Cyclone software suite.**

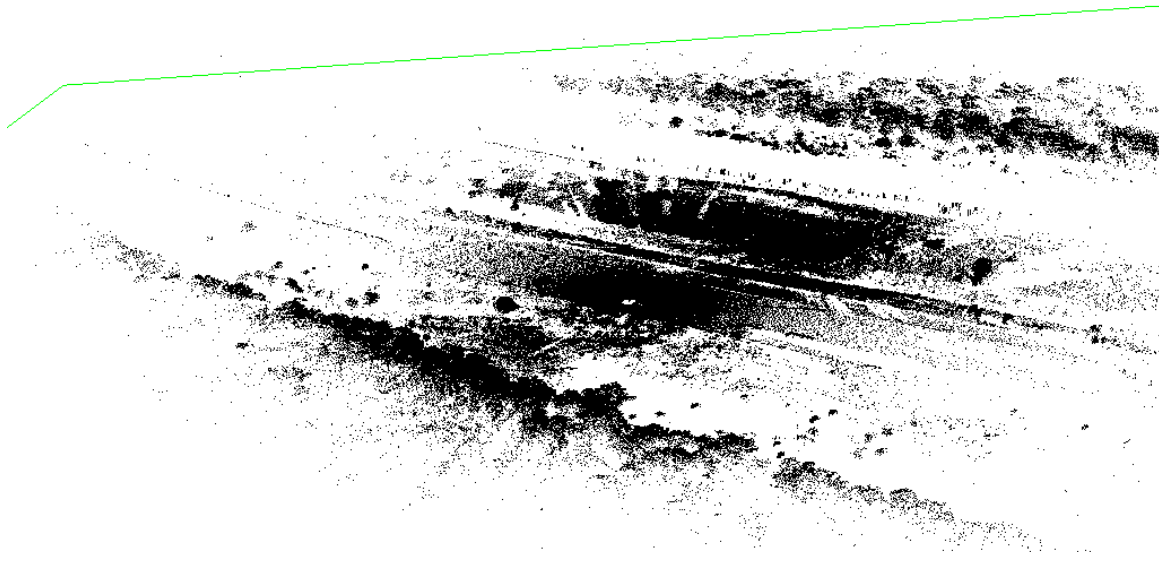


**Figure A.2. Unified point cloud (.las) as viewed in lastools lasview.exe.**

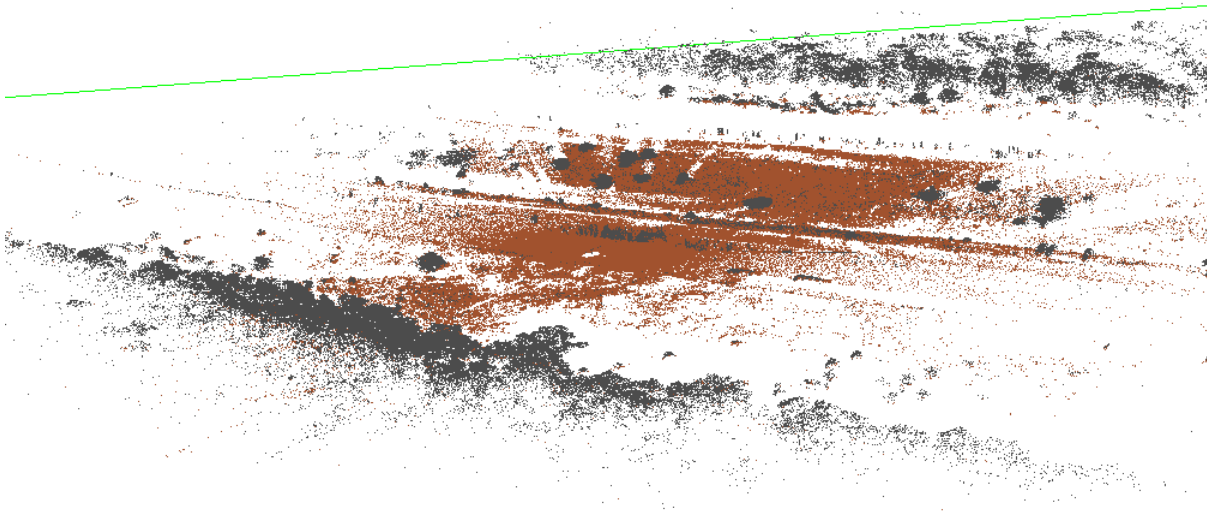


**Figure A.3. Both vegetation and non-vegetative points.**



**Figure A.4. Ground point cloud after separation.**

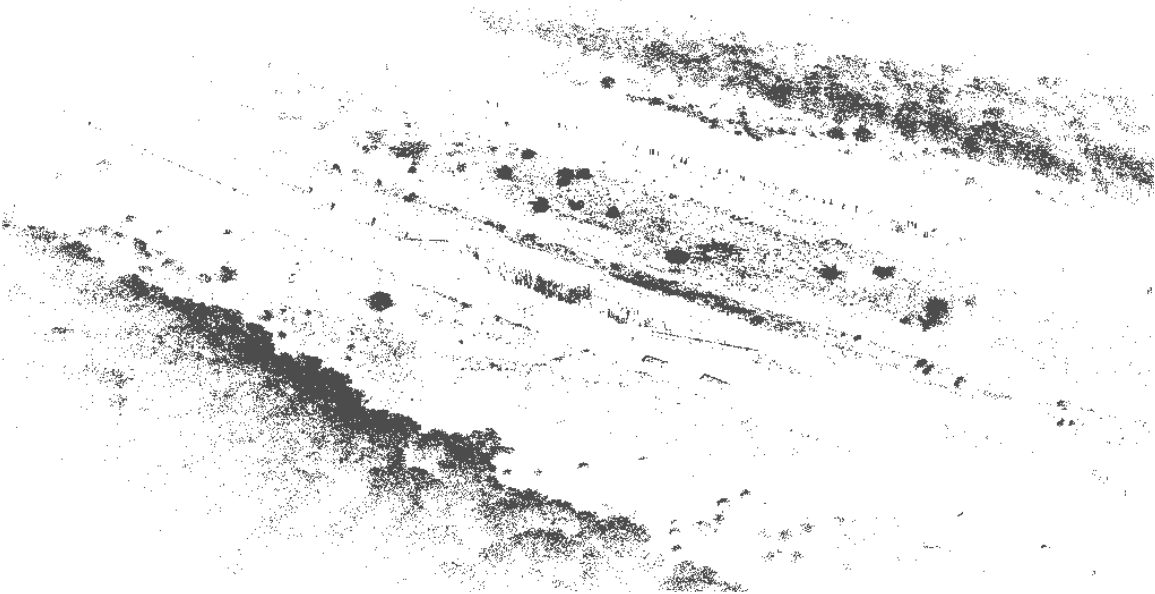


**Figure A.5. Vegetation points after separation**



**Figure A.6. Ground point cloud after thinning.**